

## Hydrous minerals on Mars as seen by the CRISM and OMEGA imaging spectrometers: Updated global view

J. Carter,<sup>1,2\*</sup> F. Poulet,<sup>2</sup> J.-P. Bibring,<sup>2</sup> N. Mangold,<sup>3</sup> and S. Murchie<sup>4</sup>

Received 31 May 2012; revised 1 November 2012; accepted 12 December 2012.

[1] The surface of Mars has preserved the record of early environments in which its basaltic crust was altered by liquid water. These aqueous environments have survived in the form of hydrological morphologies and alteration minerals, including clays and hydrated salts. Because these minerals probe on Earth aqueous environments compatible with biotic activity, understanding their formation processes on Mars is of great exobiological relevance and also offers insight into Earth's now erased ancient water environments. Using remote sensing, we conducted a large-scale investigation of the distribution, composition, age, and geomorphic settings of hydrous minerals on Mars, providing a sharpened global view of the early aqueous environments and their evolution with time. Aqueous alteration seems to have produced clays on a planetary scale but these are found to be restricted to the oldest observable terrains on Mars (~4 Gyr). However, very diverse aqueous environments have also been found which suggest widespread, complex aqueous settings from the surface to kilometric depths, and spanning over 1 Gyr. By building a robust statistical sample of detections, the global trends inferred here attempt to provide a broad view of our current understanding of hydrous minerals on Mars and provide context for more localized, in-depth analyses. Collectively, these trends suggest that at least transient conditions have existed on Mars which may have been favorable for pre-biotic to biotic activity.

**Citation:** Carter, J., F. Poulet, J.-P. Bibring, N. Mangold, and S. Murchie (2013), Hydrous minerals on Mars as seen by the CRISM and OMEGA imaging spectrometers: Updated global view, *J. Geophys. Res. Planets*, 118, doi: 10.1029/2012JE004145.

### 1. Introduction

[2] The record of episodes of early (>3 Gyr old) aqueous activity on Mars is preserved in the form of morphological features as well as in the mineralogy of the surface. Precipitation, run-off, and ponding of liquid water have shaped many structures on Mars, some of which are still preserved today albeit heavily disrupted [e.g., *Fassett and Head*, 2008b]. They are the testimony of an era when water was stable at least episodically on the surface and in the sub-surface as part of a hydrological system. The discovery of phyllosilicates, sulfate salts, and hydrated silica on Mars [*Poulet et al.*, 2005; *Gendrin et al.*, 2005; *Arvidson et al.*, 2005; *Milliken et al.*, 2008] has spawned a new era of high enthusiasm and intense scrutiny of Mars's earliest, Noachian-aged terrains. Using almost exclusively in situ measurements by the Mars Exploration Rovers and two imaging spectrometers,

OMEGA (Observatoire pour la Mineralogie, l'Eau, la Glace et l'Activite) [*Bibring et al.*, 2004] and CRISM (Compact Reconnaissance Imaging Spectrometer for Mars) [*Murchie et al.*, 2007], our view of the aqueous alteration on early Mars has considerably sharpened over the past decade. These minerals yield strong constraints on their geochemical formation settings. Placed in their geomorphic contexts, they provide unique insights into the ancient wet environments on Mars and their evolution across the eons, in the frame of the planet's global geological history. As tracers of aqueous episodes, they also constitute major exobiological targets [e.g., *Poulet et al.*, 2009] and their occurrence has been a strong driver for the choice of current and future landing sites of roving missions, including the most recent Mars Science Laboratory [*Golombek et al.*, 2012]. Martian hydrous minerals are also considered to offer a unique window into Earth's pre-biotic era as Mars' oldest terrains preserved the record of geochemical conditions not dissimilar to what has been inferred for Earth [e.g., *Meunier et al.*, 2010] and which were not entirely obliterated by plate tectonics and 3 Gyr of intense hydrological and biological activity.

[3] A broad comprehension of the state and fate of water on Mars and thus of its exobiological potential has been achieved on the basis of both global investigations of the aqueous mineralogy and through many in-depth analyses of specific regions of Mars. It has been proposed that Mars

<sup>1</sup>European Southern Observatory, Santiago, Chile.

<sup>2</sup>Institut d'Astrophysique Spatiale, Universite Paris-Sud, Orsay, France.

<sup>3</sup>Laboratoire de Planetologie et Geodynamique de Nantes, Universite de Nantes, Nantes, France.

<sup>4</sup>Applied Physics Laboratory, Laurel, Maryland, USA.

Corresponding author: J. Carter, European Southern Observatory, Santiago, Chile. (jcarter@eso.org)

©2012. American Geophysical Union. All Rights Reserved.  
2169-9097/13/2012JE004145

experienced an early wet era on its surface and/or sub-surface which formed most phyllosilicates [Bibring *et al.*, 2006]. Subsequently, global geological and climatic changes led to a dry and acidic era where surface conditions only allowed the precipitation of salts and opaline silica, while the past 3 Gyr of the planet's history have experienced little to no aqueous alteration. Independently of the climatic conditions, some hydrous minerals also likely formed at depth. Within this global frame, small pockets of alteration have been found to have occurred throughout the planet's history in very diverse environments. All of these results owe a lot to Earth-based complementary approaches including field work, geochemical experiments, and laboratory measurements of analogue sites and minerals. Many questions remain unanswered however, such as the intensity and duration of Mars's subsurface and surface hydrological systems, the geochemical states, and therefore habitability conditions.

[4] The diversity and complexity of the hydrous mineralogy and corresponding geomorphic context have steadily increased over the years owing to investigations of localized alteration exposures on Mars. As a complement to these local approaches, a broader albeit coarser perspective is required to understand the global evolution of alteration in pair with the planet's climatic and geological evolution. Using early data from the OMEGA instrument, Poulet *et al.* [2007] provided the first global map of hydrated minerals on Mars. At the spatial resolution of OMEGA ( $>1.8$  km/pixel), only five regions exhibited extended hydrous mineral exposures: Terra Meridiani, the surroundings of Mawrth Vallis, Nili Fossae, the Valles Marineris canyons, and the circum-polar northern gypsum deposits. Three types of hydrous minerals were found: Fe/Mg-rich phyllosilicates (nontronite), Al-rich phyllosilicates, and hydrated sulfates. Later OMEGA-based investigations expanded the initial distribution with a few new exposures (mostly phyllosilicates) found scattered over the southern highlands, including in the Tyrrena Terra region. The diversity also increased as Al-clays were discriminated between Al-rich smectites (montmorillonite) and Al-kaolins.

[5] The orbital operations of the Mars Reconnaissance Orbiter, hosting the CRISM instrument and high-resolution imagers, have dramatically sharpened our view of hydrous minerals on Mars in terms of composition, setting, and global spatial distribution. Works by Mustard *et al.* [2008], Milliken *et al.* [2008], Ehlmann *et al.* [2009], Poulet *et al.* [2009], Murchie *et al.* [2009], Ehlmann *et al.* [2011a, 2011b], and others have revealed hundreds of hydrous mineral exposures scattered over the southern highlands, identified several new mineral phases, and found broad correlations between the composition and geomorphic context. New phases have been identified: the hydroxylated phyllosilicate prehnite, zeolites, carbonates, serpentines, and hydrated (opaline) silica. The diversity of previously found mineral groups was also expanded. In addition to hydrated sulfates (including bassanite and gypsum), the hydroxylated sulfates jarosite and alunite were also detected. Fe/Mg-rich phyllosilicates were found to be Fe-rich smectites (nontronite), Mg-rich smectite mixtures (including saponite), chlorites, and possibly mixed-layered clays (akin to corrensite). Al-phyllosilicates were found to be kaolins, smectites (akin to montmorillonite), and Al-rich micas (illite or muscovite).

[6] Hydrous minerals were found in a variety of settings as classified by Murchie *et al.* [2009]: layered phyllosilicates, phyllosilicates in intra-crater fans, plains sediments, deep phyllosilicates (in crustal outcrops or associated with impact craters), carbonate deposits, inter-crater clay-sulfate deposits, Meridiani-type layered deposits, Valley-type layered deposits, siliceous layered deposits, and gypsum plains. While some degree of arbitrary was recognized in sorting detections into these broad classes, they indicated nonetheless that orbital investigations could, by coupling imagery to spectroscopy, decipher the broad formation/transformation environments of some hydrous minerals on Mars.

[7] We present here the result of a new global investigation of hydrous minerals on Mars. A systematic approach at a global scale is applied to infer trends in the distribution, compositional diversity, geomorphic context, and timing of the hydrous mineral exposures on Mars. Like other global works, it spawned from the necessity to have a broader perspective on the alteration environments and their evolution through time than localized investigations allowed. Because the same level of detail cannot be achieved for a large sample of detections, this work not only complements these thorough local investigations but also leads to the identification of new sites of particular interest which have been put under greater scrutiny. For this global approach, we chose to concede on a detailed geomorphic analysis but performed full spectral analysis for the detection and characterization of hydrous minerals. An upcoming paper will present the results of a number of detailed regional and local scale investigations which spawn from this work and will allow us to better define the relationships between the different formation processes of hydrated mineral deposits. By building the largest set of hydrous detections on Mars to date, we can use a more robust statistical approach to infer global trends. Equally importantly, this is a single independent analysis, performed using the same detection methods and characterization strategies for the entire set allowing for more consistent and uniform comparisons among mineral deposits. This differs significantly from all previous global investigations which were based on meta-samples collected from distinct works, using different methods with variable scrutiny.

[8] In section 2.1, we present the method used to detect and characterize hydrous minerals with OMEGA and CRISM. In section 2.2, we present the data sets used to build the statistical set of detections, and in section 2.3, we discuss the numerous biases and limitations of our investigation. The results are then presented under several aspects: spatial distribution and extent of the alteration (section 3), mineralogical diversity including the detection of new hydrous minerals (section 4), age of the deposits (section 5), and broad morphological context (section 6). Our results are then compared to those previously derived from other data sets (section 7).

## 2. Data Selection, Reduction, and Biases

### 2.1. OMEGA and CRISM Observations of Hydrous Minerals

#### 2.1.1. Instrument Descriptions

[9] Mineral composition is determined using surface reflectance data from the OMEGA and CRISM imaging spectrometers [Bibring *et al.*, 2004; Murchie *et al.*, 2007]. Both instruments operate in the visible to near infrared range

(0.38–5.1  $\mu\text{m}$  sampled at 14 nm and 0.36–3.92  $\mu\text{m}$  sampled at 6.55 nm, respectively). For the purpose of this work, we only utilize the 1.1–2.65  $\mu\text{m}$  range where spectral features of hydrous minerals are found. OMEGA samples the Martian surface from  $\sim 4.1$  km/pixel down to  $\sim 350$  m/pixel, nadir-pointed. It achieved 51% coverage at samplings  $< 500$  m/pixel and near total coverage at samplings  $< 4.1$  km/pixel. CRISM has a gimbaled quasi-nadir “targeted” observation mode capable of achieving a spatial sampling down to 36 or 18 m/pixel. The combined spatial coverage of all CRISM high-resolution targeted observations amounts to less than 2% of the surface of Mars. CRISM also achieved near global coverage at lower spatial (100–200 m/pixel) and spectral ( $\sim 54$  nm) sampling in nadir-pointed survey modes.

### 2.1.2. Identification of Hydrous Minerals in the Near-Infrared Domain

[10] Hydrated minerals are detected in the 1.1–2.65  $\mu\text{m}$  range, thanks to combinations and overtones of vibrational transitions whose fundamentals occur between 2.7 and 15  $\mu\text{m}$  [e.g., Clark *et al.*, 1990; Cloutis *et al.*, 2002, 2006; Bishop *et al.*, 2008a]. The near-infrared spectrum is dominated by features associated either with  $\text{H}_2\text{O}$  or the  $\text{OH}^-$  group.  $\text{H}_2\text{O}$  is either adsorbed at the crystals’ surface, or absorbed in the inter-layers present in most hydrous silicates (H-bonded to the lattice and/or with other inter-layer water molecules). Water induces absorption bands in the 1.35–1.55, 1.85–1.98, and 2.70–2.85  $\mu\text{m}$  regions with the latter partially spilling into the studied spectral range when absorptions are strong.  $\text{OH}^-$  is found in the crystal structure of most hydrous minerals. It exhibits a stretch transition in the 1.35–1.55  $\mu\text{m}$  region and a number of additional diagnostic bands in the 2.14–2.65  $\mu\text{m}$  region due to vibrations of the X-OH bond where X is a structural cation (typically  $\text{Mg}^{2+}$ ,  $\text{Fe}^{3+}$ ,  $\text{Fe}^{2+}$ ,  $\text{Al}^{3+}$ , or  $\text{Si}^{4+}$ ). The exact positions of these additional bands are a good proxy for the cationic mineral composition. In turn the number of degrees of freedom in cation composition induces small shifts in the position and shape of the absorption bands that make it difficult to accurately predict the exact spectrum of a given hydrous mineral [e.g., Balan *et al.*, 2002]. The alternative has been to build spectral repositories of laboratory spectra where the purity of the sample can be assessed with great precision (e.g., the USGS, RELAB, and ASTER spectral libraries [Pieters, 2010; Clark, 2007; Baldridge *et al.*, 2009]). The spectra are then compared to CRISM and OMEGA spectra to attempt mineral identification. Some minerals (such as prehnite or epidote) have a sufficient number of bands in the 1.1–2.65  $\mu\text{m}$  range that unambiguously allow their identification while others are classified within broader families (e.g., Fe/Mg-rich smectites). Because the cation composition is closely related to the geochemical environment in which the mineral is formed/transformed, coarse identifications are nevertheless often sufficient to constrain their likely geochemical formation/transformation environment.

### 2.1.3. Data Reduction

[11] The OMEGA and CRISM data cubes are converted from calibrated radiance to surface reflectance in a standard two-step process accounting for photometric and atmospheric effects [e.g., Murchie *et al.*, 2009 and references therein]. We use the modified “volcano-scan” atmospheric correction from McGuire *et al.* [2009] which removes  $\text{CO}_2$  absorption bands in the spectra. This correction does not

take into account the effects of aerosols, which cause an over/under-estimation of the mean near-infrared reflectance and induce a negative slope in the spectra [Vincendon *et al.*, 2009]. Because these effects do not induce absorption features in the studied spectral range, they are not a major issue for the detection of hydrous minerals so long as the atmospheric opacity  $\tau_{\text{NIR}}$  remains relatively low (typically  $\tau_{\text{NIR}} < 2$ ).

[12] We detect and map hydrous minerals on Mars using simple band math between spectral channels to highlight the different absorption features. This spectral criteria approach is a fast and efficient detection method. A set of spectral criteria is used allowing the identification and mapping of either broad families or individual hydrous mineral species. Any putative detection from these spectral criteria maps is verified manually.

[13] Both OMEGA and CRISM exhibit a number of instrumental artifacts that affect the spectra and in turn the spectral criteria, with the risk of causing false positives and false negatives in the mineral maps. These are common to imaging spectrometers and include bad detector elements, nonlinear detector response at the percent level, spatial striping, spectral spiking, and spectral smile. Detections of hydrated minerals are further impeded by observational biases such as surface dust mantling (modifying the spectral continuum which impacts the spectral criteria), ices (contaminating mineral bands), residuals in the atmospheric correction, photometric effects (e.g., shadows), and mixtures with non-hydrated minerals. All these effects are collectively tackled by introducing a new set of data reduction strategies which allow more accurate and more sensitive detection and mapping of hydrous minerals on Mars. These are described in details in Carter *et al.* [2012c]. Here, we only utilize the end-products of these processing steps which are spectral end-members extracted from CRISM data and their corresponding maps.

## 2.2. Analysis Strategy

### 2.2.1. OMEGA Data

[14] Due to inherent differences in the spatial resolution and coverage of the OMEGA and CRISM instruments, we could not adopt the same data selection strategies. OMEGA’s lower spatial resolution and greater spatial coverage are used to screen the planet at a global scale for extended exposures of hydrous minerals (larger than several tens to hundreds of square kilometers). The first approach to OMEGA data is an extension to that used by Poulet *et al.* [2007]: we automatically scanned the entire data set (taken from orbit insertion in late 2003 to the failure of the cooler of the 1–2.6  $\mu\text{m}$  channel in September 2010) at all spatial resolutions in search of signatures at 1.9  $\mu\text{m}$ . This corresponds to 6500 observations within which we selected hundreds of clusters of few (typically  $< 10$ ) pixels displaying a 1.9  $\mu\text{m}$  absorption depth above the conservative threshold of 2%. The detections were then investigated manually for confirmation. We find  $\sim 40$  new hydrous mineral detections that are mainly concentrated in the Terra Sirenum, Thaumasia Planum, and Terra Tyrrhena regions.

[15] Following this first screening, OMEGA data were used to achieve a more thorough investigation of three regions on Mars: Terra Sirenum, Thaumasia Planum, and Terra Tyrrhena. We processed all relevant data acquired until September 2010 in search for hydrous minerals through

several absorption bands (at  $\sim 1.9$ ,  $\sim 2.2$ ,  $\sim 2.3$ , and  $\sim 2.4$   $\mu\text{m}$ s) and with a lower detection threshold (typically 0–1%) depending on the observation. Each detection was then investigated manually for confirmation. A manual verification is always paramount as a trained user can more reliably identify diagnostic mineral signatures while discarding false positives induced by artifacts or contaminants in the spectra and mineral maps. A manual verification of the spectra usually involves taking several spectral ratios between different pixels (or groups of pixels) from the region of interest and from a neighboring, non-hydrated region, thus highlighting the mineral signatures. It also enables to assess the presence of species through a set of signatures rather than a single absorption band, increasing the robustness of the detection. Mineral maps are also screened for non-physical features in them or the presence of known, non-hydrated minerals which can induce false positives. This approach led to the identification of  $\sim 400$  new hydrous mineral exposures on Mars, some of which had a 1.9  $\mu\text{m}$  band too weak to be detectable or missing altogether. This tenfold increase in detections shows the limitation of the automated global screening method. The manual screening is too time consuming to be applied to the entire surface of Mars, hence our “two-step” approach.

### 2.2.2. CRISM Data

[16] The CRISM has surveyed the near entirety of the surface at a spatial resolution of 100–200 m/pixel using a low spectral sampling of  $\sim 56$  nm. This spectral sampling is however too low to precisely identify most hydrous minerals on Mars (see section 2.3.1), and therefore these observations have minimally been used in this work. Instead, we use CRISM targeted observations (better than 36 m/pixel) as the major source of data of our investigation. These observations can identify exposures smaller than 1  $\text{km}^2$ . Spatial coverage in this mode is very low ( $< 2\%$ ) and inhomogeneous, and this needs to be taken into account when deriving the global distribution of hydrous minerals on Mars (see section 2.3.2). Given the amount and the complexity of data, it is not possible to perform a blind survey of the entire data set. A choice of the targets must thus be made based on scientific criteria. Specifically, 2220 targeted CRISM observations are analyzed here (out of  $\sim 9500$  for the whole data set at the time of this study) based on the criteria below. For each criterion is specified the fraction (in percent) of the 2200 observations which was selected according to this criterion. This fraction is a crude estimate to provide a broad assessment of potential biases in the selection method:

[17] (1) Regional investigations. All available data within a given region are analyzed. These include the greater Tyrhena Terra region, all northern plain craters with diameters  $> 10$  km and a number of smaller sites scattered throughout the planet (e.g., intra-crater deposits in Terra Sirenum, dissected terrain in Thaumasia Planum, and high thermal inertia outcrops in Margaritifer Terra). Approximately 50–60% of the detections are the result of these thorough regional investigations.

[18] (2) Targets of opportunity. A spot at the surface of Mars is observed based on its morphology or other properties such as thermal inertia, or characterized as potential landing site of future missions. Approximately 30–40% of the detections are the result from the investigation of such targets of opportunity.

[19] (3) Confirmation or sharpening of a previous OMEGA detection of hydrous mineral. Every OMEGA-based detection of a hydrous mineral exposure was subsequently submitted for targeting with CRISM. Roughly 30–50% of these were acquired. Approximately 15% of identified hydrous mineral exposures come from the confirmation of OMEGA detections.

[20] (4) Confirmation of a detection of hydrous minerals made by other orbital instruments (TES/THEMIS) or by landed missions (the MERs). These account for a small fraction ( $\sim 1\%$ ) of the detection set.

[21] (5) Additionally, about 70 detections were made based on CRISM multi-spectral observations (100–200 m/pixel), mostly to provide coverage around targeted observations.

[22] The instrument targeting and our data selection strategies suffer from a major bias: units with no marked geomorphology will be less targeted than those with an interesting one. For example, the northern plains and dusty regions of Mars are less covered than exposed Noachian rocky outcrops; central peaks of craters and large scale features (e.g., scopolus, fossae) are more targeted than Noachian plains. While we have analyzed observations from all major units on Mars, including those with few CRISM targets, most of the targets covered the southern Noachian highlands, thus biasing the spatial distribution. This issue will be addressed in more detail in section 2.3.2. As will be explained in section 2.2.4, four extensive hydrous mineral-bearing deposits were ignored from this data selection process: little to no CRISM observations have been analyzed in the regions of Sinus Meridiani, Valles Marineris, Nili Fossae, and the northern circum-polar gypsum deposits.

### 2.2.3. Polar and Atmospheric Processes

[23] Polar and atmospheric processes are an important source of bias.  $\text{CO}_2$  and  $\text{H}_2\text{O}$  ice frosts occur in winter poleward of  $\sim 45^\circ$ , restricting the observational periods and spatial coverage of these regions. Ice coverage poleward of  $\pm 60^\circ$  precludes a global investigation of peri-polar and polar terrains: we therefore restricted our investigation to latitudes equatorward of ( $-60^\circ$ ,  $+60^\circ$ ). The lowest regions of Mars have the longest atmospheric path length and are subjected to high aerosol opacity. The Hellas and Argyre basins are particularly affected by high opacity and surface frosts, and the investigation of their surface composition is difficult, resulting in a bias in the distribution of hydrous minerals there. Because of the high temporal and spatial variability of aerosols and frosts on Mars, we do not systematically screen out non-polar observations based on their season, latitude, or altitude. Rejection of frost-covered or high-opacity observations is done on a case-by-case basis.

### 2.2.4. Global Distribution: Merging the Two Data Sets

[24] From the identification of individual exposures of hydrous minerals, we infer a number of actual detections of hydrous mineral-bearing sites. An individual mineral exposure is defined by a group of continuous or loosely continuous pixels which collectively show the same spectral feature corresponding to a given hydrous mineral. When it can be ascertained that two such groups of pixels are spatially disconnected, then the exposures are considered as two separate sites. Within each site, independently of the number of hydrous mineral species found, only one detection is counted. This is because we consider that two or more minerals found within the same pixel or small group

of pixels are likely genetically connected and belong to a single site. This rule is applied for all exposures identified with OMEGA. Because CRISM has a much smaller field of view, we consider that all the exposures identified within each targeted observation are likely genetically linked in most cases and therefore only account for one detection (whether they appear spatially connected or not and regardless of the number of different mineral species). Overlapping detections of CRISM and/or OMEGA are also only counted as one detection. Taking this into account, the total number of independent mineral exposures on Mars amounts in fact to about 10,000.

[25] Figure 1 shows the location of all detections of hydrous mineral sites on Mars from this investigation. A total of 1230 sites are shown, 260 were made solely with OMEGA (blue dots), 800 were made solely with CRISM (red dots), and 170 were co-detected by both instruments (orange dots).

[26] As mentioned previously, our study excludes four geographical areas of Mars which exhibit extensive hydrous mineral exposures: Sinus Meridiani, Valles Marineris (and surrounding chaos), Nili Fossae, and the northern circum-polar gypsum dune deposits. These regions were amongst the first detected on Mars and have been put under intense scrutiny over the past years (totaling tens of publications [e.g. Roach, 2009; Ehlmann et al., 2009; Mangold et al., 2008; Poulet et al., 2007; Massé et al., 2010]), so that our broad-scale approach would little contribute to bettering our knowledge of these regions. The mineralogy found there is also quite different (especially the sulfate-rich ones) to that found in our global investigation. Because these are spatially extensive deposits which have been heavily targeted with OMEGA and CRISM, had our blind survey included these regions, a high statistical weight would have unavoidably been placed upon them, thus biasing our study. To preclude

such bias, very few OMEGA and CRISM observations were analyzed in these regions and all the statistics presented hereafter which are solely based on CRISM data will not be preferentially based on them. For similar reason, the major and continuous deposit of Mawrth Vallis as mapped by Poulet et al. [2005] is also excluded. We nevertheless consider numerous small exposures around the extensive deposit, increasing significantly the number of detections reported in this region by Noe Dobrea et al., [2010]. For the sake of completeness, an updated OMEGA map of the three low-latitude extensive deposits (Sinus Meridiani, Valles Marineris, and Nili Fossae) is nevertheless mapped in dark blue in Figure 1 which gives a good estimate of their spatial extent.

[27] This map is hence a collection of data with different spectral samplings ( $\sim 6.5\text{--}14\text{ nm}$ ) and very diverse spatial binnings: from 18 m/pixel to 4.1 km/pixel. This multi-scale approach is however very useful as it allows the identification of major (extended) exposures as well as exposures restricted to very small units (e.g., crater central peaks, scarps). Using CRISM as a complement to OMEGA also allows refining the spectral diversity and context of the major exposures identified with OMEGA. The next section will investigate the biases induced by the heterogeneities in spatial and spectral resolutions.

## 2.3. Biases and Limitations

### 2.3.1. Spectral Resolution

[28] The full width at half maximum (FWHM) of diagnostic bands of interest of hydrous minerals ranges between 9 (respectively 5) and 15 spectels (respectively 8) for CRISM (respectively for OMEGA). There are always enough spectral channels on which to compute the spectral continuum so that it is not a limiting factor in our detection capability. If the

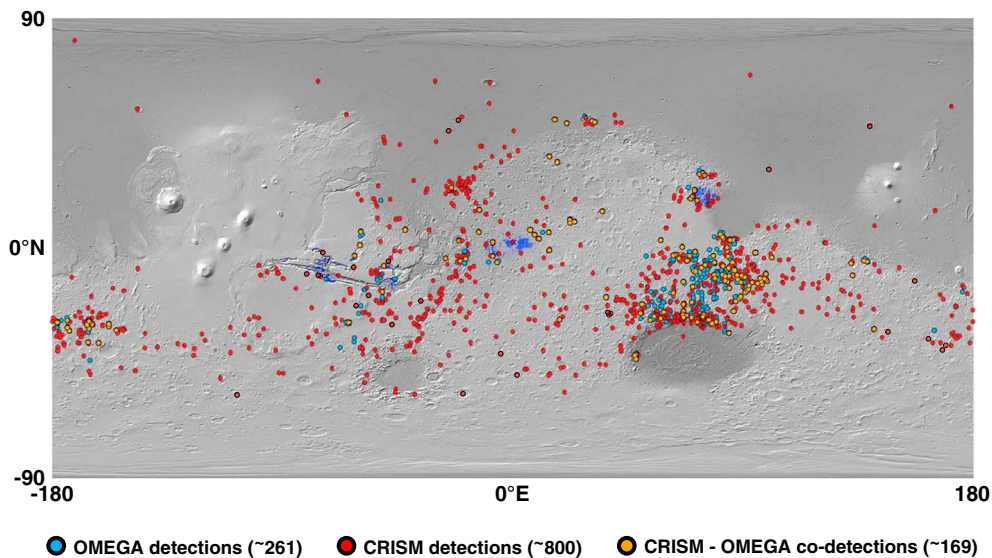


**Figure 1.** Global map of hydrous mineral detections on Mars. Each dot indicates the position of a hydrous mineral exposure detected either by CRISM (red), OMEGA (blue) or jointly by both instruments (orange). Only one exposure is counted per CRISM observation regardless of the number of different hydrous mineral species found (see text). Overlapping detections are also excluded. In dark blue are OMEGA maps of hydrous minerals in Valles Marineris, Sinus Meridiani, and Nili Fossae, which will be hereafter excluded from this study.

spectral resolution was a limiting factor, we would expect that minerals whose diagnostic band has the narrowest FWHM would be relatively less frequently detected with OMEGA than with CRISM. Although we do find a relative increase in the number of detections of every hydrous mineral between OMEGA and CRISM, we found no apparent correlation with the various diagnostic bands' FWHM. Consequently, the lower spectral resolution of OMEGA does not induce a major source of bias in the detections compared to CRISM.

[29] Conversely, the lower spectral binning of multi-spectral CRISM observations ( $\sim 56$  nm), leads to an FWHM  $\leq 4$  spectels for most hydrous minerals, which makes more difficult their detection and the determination of their precise mineralogy. Some minerals such as kaolins and Al-clays have an FWHM of only 2 spectels. We find that only Fe/Mg clays and chlorites/prehnite can be confidently identified using these observations.

### 2.3.2. Spatial Resolution

[30] Figure 2a shows a histogram of the number of analyzed observations and detections of hydrous minerals according to the spatial sampling of the observation modes: 18 m/pixel (CRISM "FRT"s), 36 m/pixel (CRISM "HRL"s and "HRS"s), 200 m/pixel (CRISM "MSP"s), 350 m/pixel (OMEGA "mode 16"), 720 m/pixel (OMEGA "mode 32"), 1500 m/pixel (OMEGA "mode 64") and 4000 m/pixel (OMEGA "mode 128"). These are average samplings based on the instrument footprint and vary with the spacecraft altitude for OMEGA. While the spatial resolutions are complementary as mentioned previously, most of the detections are done thanks to the highest resolution of CRISM.

[31] To better quantify the effect of spatial sampling, we compare the number of detections normalized by the surface coverage of Mars covered at each spatial resolution. The surface coverage at each resolution is simply the average footprint (in  $\text{km}^2$ ) at each resolution times the number of analyzed observations. Figure 2b shows a decrease in detection density with decreasing spatial sampling roughly following a power-law trend. The MSP 200 m/pixel observations

deviate somewhat from this power-law trend, but this is likely due to statistical errors since only a very small sample of these observations has been taken into account. This trend clearly demonstrates that the detection capabilities are limited by the spatial resolution of the observations, which in turn indicates that spots with hydrous minerals as small as the smallest footprint ( $\sim 20$  m) can be detected.

### 2.3.3. Spatial Coverage

[32] Because OMEGA observations cover a significant fraction of the planet at low resolution but represent only a minor fraction of the detection sample, we here focus on CRISM targeted observations. The resulting distribution of hydrous minerals on Mars is patchy and may not be representative of the extent of the alteration. Two artifacts affect the distribution of hydrous minerals. First, many of the hydrated deposits detectable at the high spatial resolution of CRISM are surely left out in the 98% of the surface not observed. Second, some regions have been investigated more than others, yielding more detections than other regions less well studied. To tackle these effects, we map the detection rate surface density. It is simply the number of detections divided by the number of analyzed observations within a unit area taken as one square degree. Wherever the statistical sample of observations and detections is large enough, we consider the detection rate density to be a reliable proxy for the regional extent of surviving surface covered in alteration minerals. However, as a statistical measurement, it cannot be used to infer small-scale variations in the extent of altered surface. Figure 5a shows the surface density of observations. We consider the density to be statistically reliable in non-polar regions except for NW Tharsis Planum, where too few observations have been analyzed. Results are discussed in section 3.

[33] As discussed in section 2.3.1, multi-spectral CRISM observations are mostly discarded because of their low spectral sampling. These observations can still be useful to identify the large spectral  $2.3 \mu\text{m}$  drop of Fe/Mg clays and chlorites as shown in Figure 3. In this area (northern Hellas

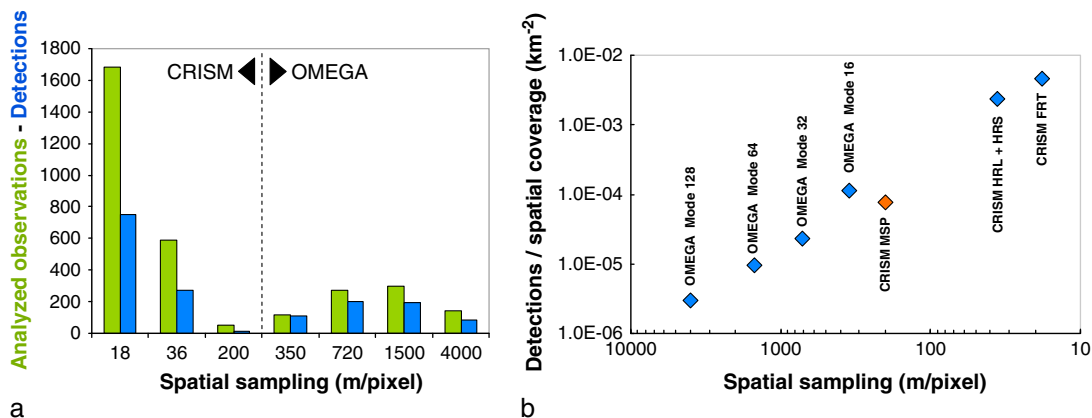


**Figure 2.** (a) Number of analyzed observations (green) and detections (blue) according to spatial resolution. (b) Detection rate (detections per observations analyzed) normalized by the surface coverage at each spatial resolution. For each of the seven instrument observing modes (CRISM FRT, HRL + HRS, MSP observations, and OMEGA modes "16," "32," "64," "128" observations), we calculated their average pixel size in meters on the Martian surface and average surface coverage. The total surface coverage for each mode is simply its average surface coverage multiplied by the number of observations using this mode in our sample.

province), the spatial distribution of Fe/Mg phyllosilicates is inferred using 16 CRISM targeted observations and seven multi-spectral observations (vertical swaths). Extensive clay exposures are identified thanks to the MSP observations, which expand the fraction of altered surface mapped in the area by an order of magnitude. Similar results for Fe/Mg clays were obtained in the northern Tyrrhena Terra region by *Mustard et al.*, [2008] and in Valles Marineris by *Murchie et al.*, [2009]. A global investigation using the MSP products should hence drastically increase the number of Fe/Mg clay exposures on Mars.

#### 2.3.4. Observational Biases

[34] The surface dust on Mars mostly comprises of iron-bearing, anhydrous silicate material. It is a major source of bias as a dust mantling thicker than a few tens to hundreds of micrometers can mask entirely the underlying rock composition [e.g., *Poulet et al.*, 2007 and references therein]. As a result, an important fraction of the Martian surface is not accessible to remote sensing in the near infrared. To assess the surface dust coverage, we use a global map of nano-phase ferric oxides based on OMEGA data [*Ody et al.*, 2012], based on the slope of the right wing of the  $\text{Fe}^{3+}$  electronic transition band between  $\sim 0.78$  and  $\sim 0.9 \mu\text{m}$ . The ferric oxides absorbed in the visible spectrum and strong absorptions yielding an OMEGA criterion value  $\geq 1$  have been considered a good proxy for the presence of surface dust [*Poulet et al.*, 2007], in agreement with TES-based maps [*Ruff and Christensen*, 2002]. Because the OMEGA-based dust map only achieved  $\sim 88\%$  coverage of the planet, we needed to infill the missing data to accurately compare with the hydrous mineral detection sample.

[35] The dust index map alongside the detections are shown in Figure 4a. A good spatial anti-correlation between dusty regions and the location of hydrous mineral exposures is observed. Another way to represent this trend is to plot the number of analyzed CRISM observations as a

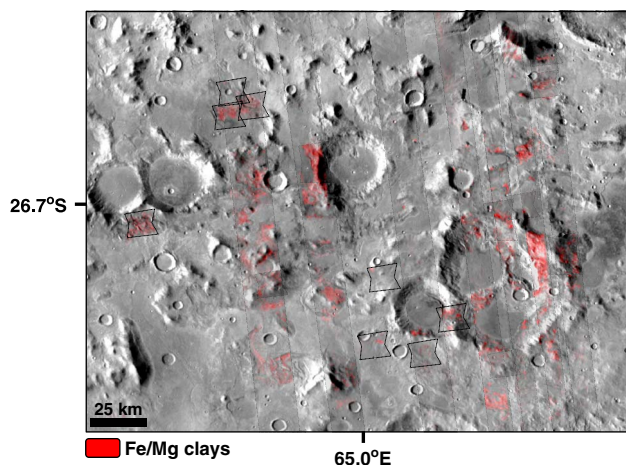


**Figure 3.** Mosaic of CRISM observations of Fe/Mg clays mapped in red in the northern Hellas province. The vertical swaths are the footprints of CRISM multispectral (MSP) observations while the smaller polygons are those of targeted observations. Background is THEMIS IR daytime (100 m/pixel) mosaic.

function of the dust index (Figure 4b). Most of detections occur at an index around 0.95 (dust-free), and their number rapidly decreases for higher values. Figure 4c shows the evolution of the detection rate normalized by the surface at each given dust index. A very sharp decrease in detection rates with higher dust index values is observed, which confirms the very strong effect of dust in hindering the detections even at low dust values ( $< 1$ ). However, one should not conclude from the lack of detection of hydrous minerals in dust-covered areas that the immediate subsurface is altered.

#### 2.3.5. Instrumental Biases

[36] The degradation of CRISM performances with time affected the detection of hydrous minerals. Due to detector aging but mostly due to cooling issues which have led to an increase of the detector temperature, the spectral noise in observations has risen over time. We estimated the spectral noise in each observation by calculating the standard deviation of a featureless portion of the spectrum between  $1.69$  and  $1.87 \mu\text{m}$  that was continuum removed and de-spiked. The average  $\sigma$  at the beginning of the mission was about 0.005. It increased by 30% to an average 0.0065 in late 2007. As of mid-2009, spectral noise increased sensibly to values around  $\sim 0.010$ , noticeably degrading data quality. This increase of spectral noise with time is independent of observational effects such as solar illumination, surface albedo, or atmospheric opacity. As expected, a slight relative decrease in detections was observed for higher noise levels. However, high spectral noise observations constitute only a small fraction of the data set used in this study, leading to an estimated  $\sim 5\%$  of missing detections. We also investigated the correlation of detection rates with solar longitude and found none, indicating that seasonal effects and solar illumination do not significantly bias the sample.

#### 2.3.6. Intrinsic Biases

[37] There are other biases intrinsic to the mineral exposures themselves. In particular, the diagnostic absorption bands have a varying depth from one species to another one and can be contaminated by other bands or artifacts. This selectively affects some hydrous minerals. For example, Al-rich micas have bands that overlap those of Al and Fe/Mg smectites, possibly leading to some mis-identifications. Fe/Mg-rich micas have too few and too shallow specific bands to allow their definite identification.

[38] The typical size of the hydrous mineral exposures is also a key factor as smaller exposures have fewer pixels to average on and result in lower S/N spectra, and hence are harder to detect. Epidote for example is a rare phase on Mars and is only found in very small exposures (a few CRISM pixels). Al-rich clay exposures are on average an order of magnitude smaller than Fe/Mg clay exposures. Their smaller exposure sizes result in lower S/N spectra and diminish their detectability from orbit. These sources of errors place varying limitations on our detection capability.

## 3. Spatial Distribution

### 3.1. Global-Scale Distribution

[39] As discussed in section 2.3.2, we investigate the global scale distribution of hydrous minerals by looking at the CRISM detection rate surface density (number of

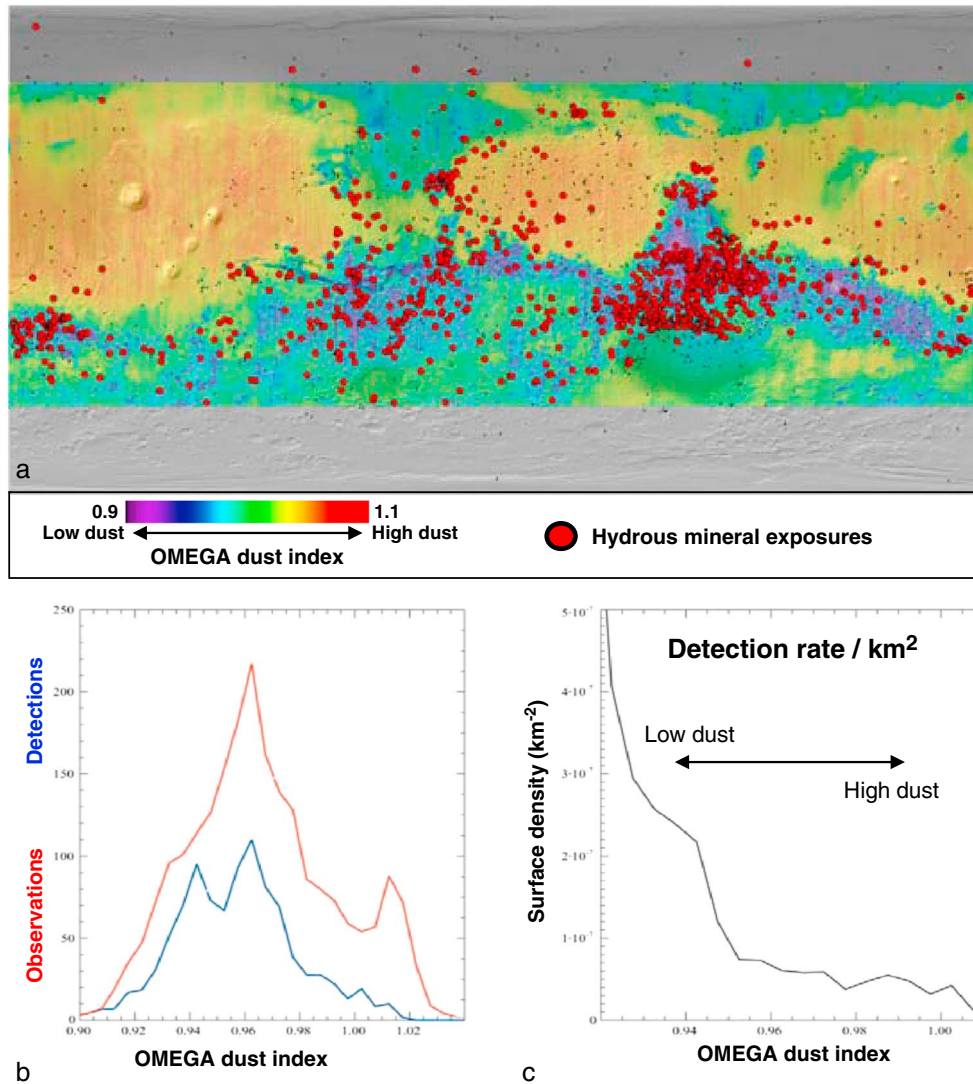


**Figure 4.** Surface dust and hydrous mineral detections. (a) The color map shows the surface dust abundance derived from the OMEGA nanophase ferric oxides criterion [Ody *et al.*, 2012]. Low or no dust regions have criterion values  $<1$  (blue tones) while high dust areas are in yellow/orange tones. CRISM and OMEGA detections of hydrous mineral exposures are shown in red circles and the black dots show the locations of all analyzed CRISM observations. Background is a MOLA composite of altimetry and hillshade. (b) Histogram of CRISM analyzed observations (red) and detections (blue) as a function of the OMEGA dust index. (c) Histogram of detection rates per surface area as a function of the dust index.

detections per observations analyzed per unit area). Results are shown in Figure 5c. To the first order, the detection rate is homogenous in the highlands, with values mostly between 0.5 and 1. There are three major regions depleted in detections: (1) the NE Arabia Terra region where high dust precludes many identifications (Figure 4); (2) the northern Tharsis plateau and other volcanic provinces (Tyrrhena Patera, Appolinaris Patera and Syrtis Major); dust coverage in Tharsis combined with the analysis of few observations does not allow us to accurately infer the surface density there. Very few detections are found in volcanic units; Syrtis Major has a few detections [Skok *et al.*, 2010] but its artificially high detection rate density on the map is mostly due to its proximity to highly altered terrains in Nili Fossae and west Lybia Montes; (3) and the northern plains, due to dust coverage and resurfacing processes: the northern plains

are however not devoid of signatures as discussed in Carter *et al.* [2010] and in section 3.2. It can be also noted that the surface density remains high down to southern latitudes ( $50\text{--}60^\circ$ ) where polar processes preclude detections more to the south. From section 2.3.2 (Figure 2), we inferred that the highest surface density of detections is achieved with the CRISM FRT observations and amounts to  $0.0045$  detections per  $\text{km}^2$ . The average size of the hydrous mineral exposures at this scale is roughly  $4 \text{ km}^2$  and hence the fraction of surface covered with alteration minerals reaches about 1.8%. This fraction is however calculated on all terrains on Mars. By sampling only dust-free (mostly Noachian-aged) units, we find the surviving fraction to be around 3.4%. This was calculated by keeping an average exposure size of  $4 \text{ km}^2$  but with a detection rate of 0.7 detection per observation corresponding to an OMEGA dust index  $<0.95$  in Figure 4.

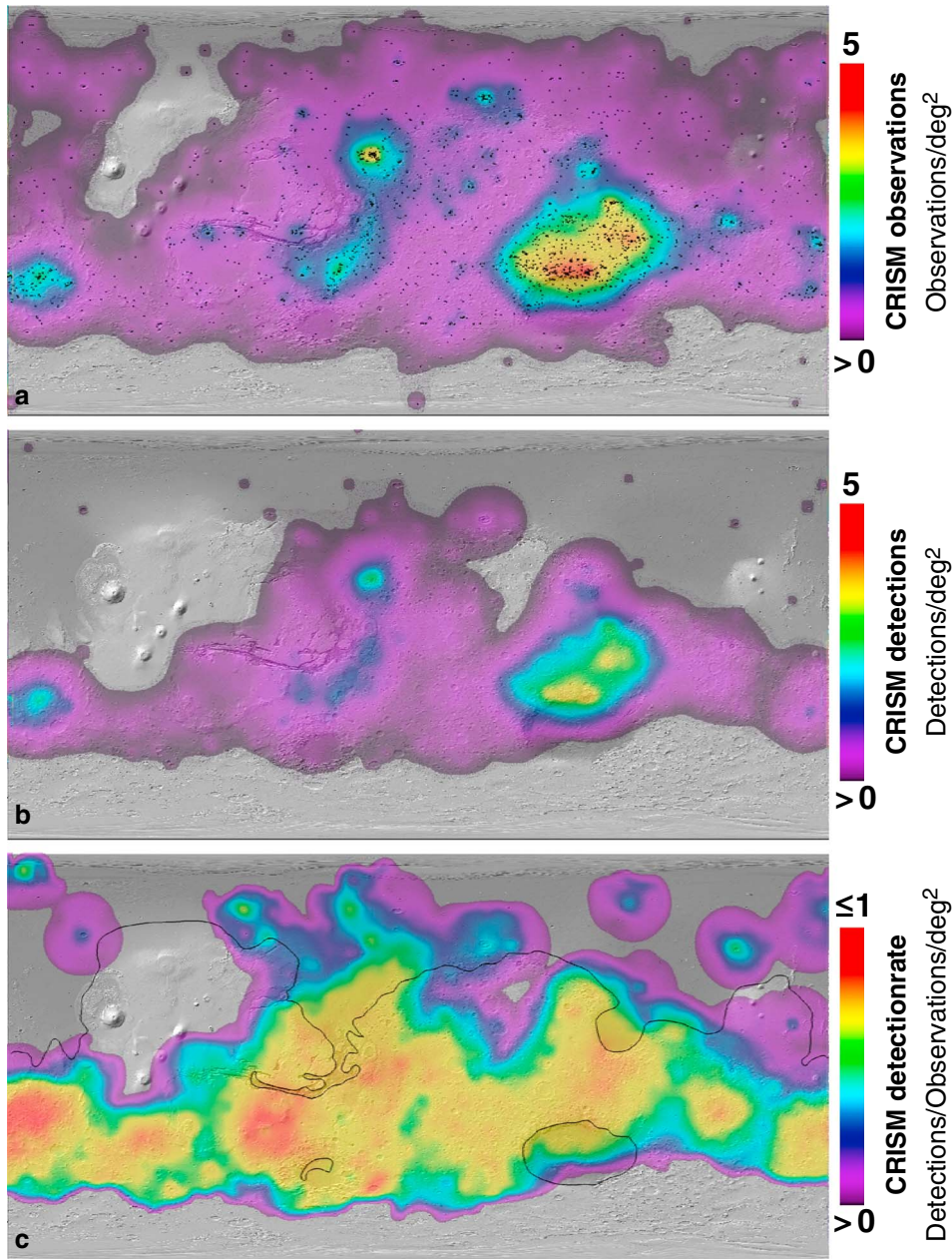


**Figure 5.** (a) Surface density of analyzed CRISM observations. The black dots show the location of the individual observations on the basis of which is derived the surface density. (b) Surface density of analyzed CRISM observations that yield detections of hydrous minerals. (c) Surface density of CRISM detection rate (detections per observations analyzed). The black line is a smoothed -3000 m altitude contour. Background is a grey-scale MOLA composite of altimetry and hillshade.

A very rough order of magnitude of the amount of water stored in hydrated minerals can be inferred from this evaluation: supposing this fraction (3%) accounts for the entire Mars surface, down to a depth of 10 km (the deepest high pressure species found, see below), with a 10% water fraction stored in these minerals, it corresponds to  $\sim 30$  m of equivalent water layer height.

### 3.2. The Northern Lowlands of Mars

[40] By studying craters of the northern plains, it was inferred in *Carter et al.* [2010] that the Noachian basement

was indeed altered to phyllosilicates. Using the excavation depth-to-diameter relation from *Baratoux et al.* [2007],  $d_{exc} = 0.109D^{0.872}$ , we find that craters with diameters  $D > 10\text{--}15$  km can safely be considered large enough to have brought up to the surface older material buried under the infilling. A sample of 100 craters was studied and to date between 15 and 19 of them have been found to display hydrous minerals (this number depends if the arbitrary boundary for the plains is taken at altitudes  $-3000$  m or  $-2000$  m). These are shown as red dots in Figure 6. As discussed in *Carter et al.* [2010], there is strong evidence that many craters

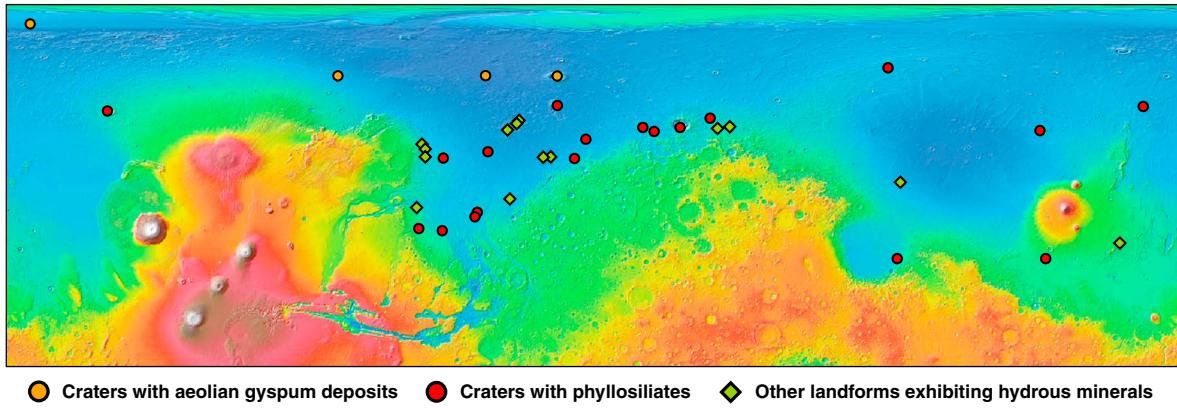


**Figure 6.** Detections of hydrous minerals in the northern plains of Mars.

indeed excavated hydrous minerals from a presumably Noachian-aged basement and did not cause the formation of hydrous minerals in post-impact hydrothermal systems. Also, a similar mineral diversity is found excavated from this basement compared to the southern highlands, possibly corresponding to a northern crust. The presence of Al-rich species, if indeed it corresponds to a later alteration episode, indicates that this process occurred before the infilling of the plains, which did not modify significantly the structure and composition of the phyllosilicates.

[41] No hydrous minerals have been detected in craters small enough to have excavated material only from the younger infilling of these northern plains. However, hydrous minerals have been detected in a few other types of settings of the northern plains. Fourteen new exposures are reported here (green diamonds in Figure 6), they comprise of buttes, cones and elongated structures (some of which are inverted channels) and are found in terrains dated from the Noachian to the Amazonian:

[42] (1) The exposure with the youngest unit age is a series of small cones and dykes or fractures which have been identified thanks to a dust-free window in the Utopia Rupes

region, in a unit of Amazonian age. Both opaline silica and zeolites (or alternatively sulfates) are found there as shown in Figure 7. Zeolites are found mainly on the butte that could constitute a small volcano, as suggested by the presence of radial patterns resembling lava flows, to the southeast especially. Silica is found on an elongated structure which is either a dyke or a structural horst. Of interest is the presence of two small cones exposed in the NE corner displaying opaline silica. Such small cones on Mars have been interpreted either as volcanic vents or mud volcanoes [e.g., Allen, 1979; Farrand et al., 2005]. In both cases, the observation of opaline silica pleads for a local fluid circulation inside a hydrothermal context consistent with volcano-ice interactions as predicted by previous studies [Allen, 1979; McGill, 2002; Farrand et al., 2005].

[43] (2) Six exposures are elongated structures, possible flow features (including inverted channels) of sedimentary or volcanic origin which exhibit Fe/Mg phyllosilicates signatures. They are found in units of SE Acidalia Planum, Cydonia Mensae, and south Acidalia Planitia. These units are dated to the Hesperian era.

[44] (3) Four exposures are small buttes in Chryse Planitia, north of Deuteronilus, and Protonilus Mensae. These are

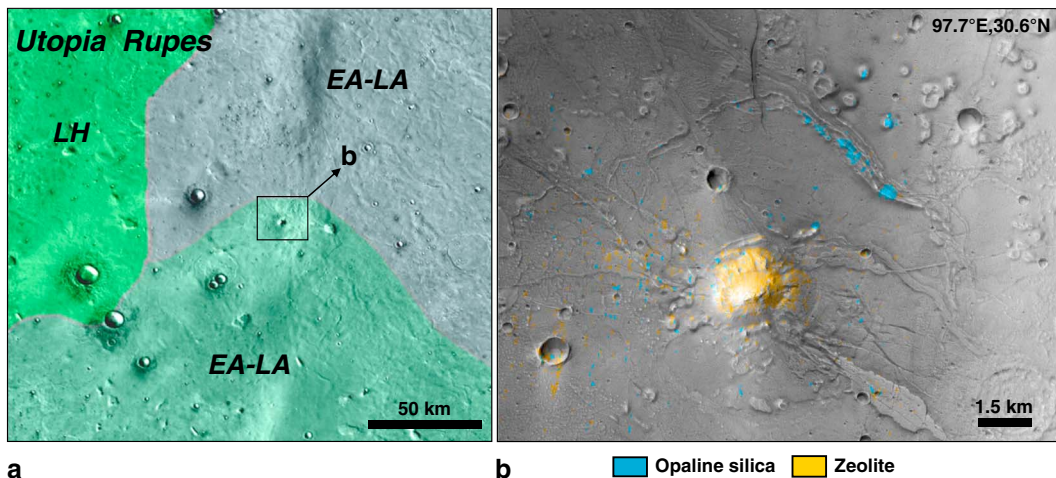


**Figure 7.** Detections of hydrous minerals in Amazonian-aged terrains of Utopia Rupes in the northern plains of Mars. (a) THEMIS mapping overlain by the geological map of Tanaka et al. [2005] of Utopia Rupes. (b) HiRISE close-up and CRISM mineral mapping in Utopia Rupes showing zeolites (yellow) over a butte and opaline silica (blue) over a NW-SE trending structure and two small cones. EA: Early Amazonian; LH: Late Hesperian; LA: Late Amazonian. North is up.

part of chaotic units at the dichotomy boundary and are likely eroded remnants of the highlands. Their units are also dated to the Hesperian era.

[45] (4) Four exposures of Fe/Mg phyllosilicates have been found in degraded buttes within units of Noachian and Late Noachian–Early Hesperian ages. Three are located in Acidalia Colles (see Figure 8) and the fourth one is located in the Tartarus Montes of Elysium Planitia.

[46] As a summary, the extent of preserved Noachian material in the northern lowlands is too restricted and the number of observations and detections too small to allow to infer the extent or the strength of alteration. It also cannot be compared directly to what was inferred for the southern highlands based on a much larger statistical sample. Despite these limitations, we find that

[47] (1) All observed dust-free Noachian units of the northern lowlands targeted by CRISM show phyllosilicate deposits. Some are located  $180^\circ$  apart in longitude. The only non-observed surviving Noachian-aged unit of the lowlands surrounds the Orcus Patera in Elysium Planitia. It has no observation covering it in our sample owing to the high surface dust content.

[48] (2) An important fraction of craters large enough to have excavated basement material display phyllosilicates, in a compositional suite similar to that of the southern highland craters. They are found at all longitudes and all sub-polar latitudes.

[49] (3) Small structures that cannot be dated accurately but whose ages range from the Noachian to the Amazonian are found to display hydrous minerals. Some are surface flow features. These are also found at a wide range of longitudes.

[50] (4) The Amazonian-aged unit displays a hydrous mineralogy different (no clays) than those of Hesperian to Noachian ages, but a geological context that could reveal transient Amazonian hydrothermal circulation.

## 4. Diversity of Hydrated Minerals on Mars

### 4.1. Overview

[51] Over 10 different hydrous minerals have been found on Mars, which typically form/transform in distinct

environments on Earth. Our investigation confirms the diversity of hydrous minerals found by previous investigations [e.g., Murchie *et al.*, 2009; Ehlmann *et al.*, 2009], but the number of occurrences significantly increases the statistics of the different mineral classes. To infer trends in composition, we sort our detections according to nine spectral classes: (1) Fe/Mg-rich phyllosilicates (including smectites, vermiculites, micas and mixed layered smectites/vermiculites), (2) chlorites (including chlorite and mixed layered chlorite/corrensite), (3) Al-rich smectites/micas, (4) Al-rich kaolins (kaolinite, halloysite), (5) opaline silica, (6) zeolites/sulfates, (7) serpentines/carbonates, (8) prehnite, and (9) epidote. Each class corresponds to one or several minerals with similar spectral features. Sorting detections into these spectral classes instead of specific mineral species is necessary to overcome limits in our identification capability. Some classes such as prehnite or epidote each trace a unique mineral because they have very specific absorption features, while others such as Fe/Mg phyllosilicates trace mineral families with a similar cationic content. The zeolite/sulfate class is the only one that groups minerals that formed in very different environments. This stems from the fact that many hydrated salts have their spectra dominated by  $H_2O$  bands similar to zeolites, which render their discrimination difficult. Serpentines and carbonates have broadly similar spectral features which can only be discriminated when the signal-to-noise of the observation is high enough. Both types of minerals were therefore conservatively placed in the mineral class, although they may at times form in different environments. We also find that while 51% of the CRISM observations displaying hydrous minerals only have one hydrous mineral class (usually Fe/Mg phyllosilicates), the remainder can have up to six different hydrous minerals within an observation.

[52] The number of detections for each mineral class is shown in Figure 9. Fe/Mg phyllosilicates are found to be by far the most common hydrous mineral on Mars, as they are found in 89% of all hydrous exposures. Chlorites/corrensites are the second most frequent class with a frequency around 20%, closely followed by Al-rich smectites/micas ( $\sim 18\%$ ). Except for epidote which was only found in five

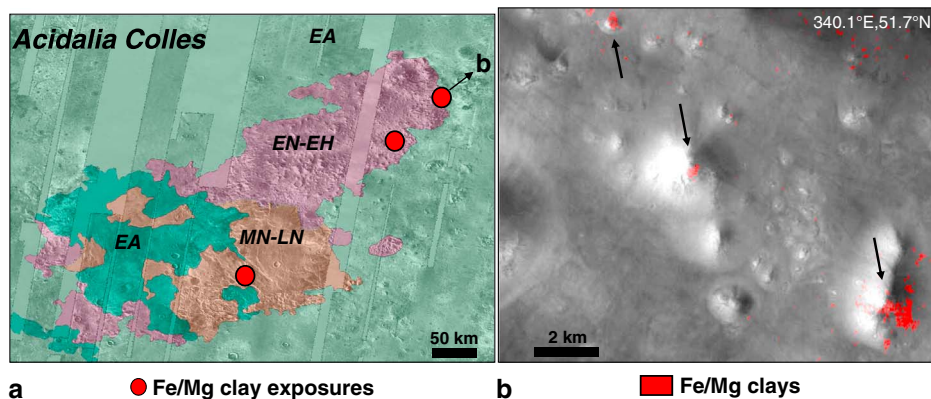


**Figure 8.** Detections of hydrous minerals in Noachian-aged terrains of Acidalia Colles in the northern plains of Mars. (a) THEMIS mapping overlay by the geological map of Tanaka *et al.* [2005] of Acidalia Colles. CRISM detections of Fe/Mg clays are shown in red. Ages are indicated for each unit. (b) CTX close-up on Noachian to Early Hesperian-aged degraded buttes displaying Fe/Mg clays (mapped in red). EA: Early Amazonian; EH: Early Hesperian; EN: Early Noachian; MN: Middle Noachian; LN: Late Noachian. North is up.

exposures, the remaining classes have a frequency between 7% and 15%. If we merge Al-rich smectites/micas and Al-rich kaolins, which are broadly found in similar environments on Earth, then Al-rich phyllosilicates become the second most common type of minerals on Mars (~33%).

#### 4.2. Detailed Spectral Analysis

[53] Table 1 summarizes the types and composition of hydrous minerals found to date on Mars using OMEGA and CRISM. We now investigate in more detail the spectral variability of some hydrous minerals detected on Mars.

##### 4.2.1. Fe/Mg Phyllosilicates

[54] The mineralogy of spectral classes exhibiting a 2.3  $\mu\text{m}$  band due to Fe and/or Mg cations bonded with hydroxyl groups consists of Fe/Mg phyllosilicates (including mixed-layered clays), Fe/Mg serpentines, and Fe/Mg carbonates. Chlorites are Al/Fe/Mg phyllosilicates which have been unambiguously identified on Mars and are little discussed in this section. It is possible to further discriminate these minerals based on both the band position and shape. Fe-rich minerals usually have bands in the range of 2.285–2.29  $\mu\text{m}$  while Mg-rich minerals have their band shifted up to 2.32/2.33  $\mu\text{m}$  [e.g., *Bishop et al.*, 2002]. The band is sharp and rather symmetrical for smectites and serpentines while it is smooth and asymmetrical in vermiculites and mixed-layered clays.

[55] Figure 10 shows several CRISM spectra representative of the diversity in position and shape of the 2.3  $\mu\text{m}$  band, excluding carbonates and serpentines. The position ranges from 2.285 to 2.32  $\mu\text{m}$ , with a shape from sharp and symmetrical to smooth and asymmetrical (close to a spectral shoulder). This indicates variability in structure and composition of the Fe/Mg phyllosilicates on Mars. The right panel shows laboratory spectra that best fit the CRISM spectra: the (Fe) end-member nontronite (2:1 smectite group), the (Mg) end-member talc (2:1 talc group), the (Mg) end-member saponite (2:1 smectite group), two (Al, Fe, Mg) vermiculites with slightly different compositions (2:1 mica group), (Al, Fe, Mg) hornblende (amphibole group), an

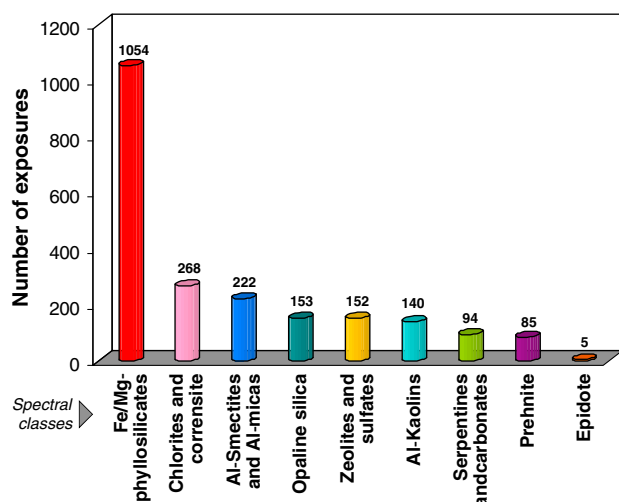


**Figure 9.** Hydrous mineral diversity on Mars. The detections are sorted into nine spectral classes that encompass the entire diversity found to-date.

(Al, Fe, Mg) chlorite, and the (Al, Fe, Mg) glauconite (2:1 mica group).

[56] The only laboratory spectrum to offer an excellent match to some CRISM spectra is that of (Fe) nontronite (top spectra in Figure 10b). Nontronite was definitely identified as early as the first OMEGA detections of clays on Mars [*Poulet et al.*, 2005], further confirmed with CRISM [e.g., *Bishop et al.*, 2008b]. (Mg) saponite has been proposed in a number of studies [e.g., *Mustard et al.*, 2008; *Ehlmann et al.*, 2009] but never proved to be a perfect match to CRISM spectra. Although never found totally pure, this phase was proposed to be one of the main components of the majority of Fe/Mg phyllosilicates on Mars [e.g., *Mustard et al.*, 2008]. Our investigation yields the same results. As proposed by several studies [e.g., *Milliken et al.*, 2010], mixed layer clays dominated by saponite are also a possibility but we lack laboratory spectra to explore this possibility further. (Mg) talc is also a possibility in some cases but while the 2.2–2.4  $\mu\text{m}$  bands are a good match to some CRISM spectra, the overall spectral shape is inconsistent with Martian spectra. Chlorites, micas (e.g., glauconite), and amphiboles (e.g., hornblende) are also a possibility to explain some features of the CRISM spectra but require a mixture with saponite. This possibility is explored below. Finally, vermiculite, an alteration mineral of biotite micas in basalts provides the best overall match to most CRISM spectra of Fe/Mg phyllosilicates: (i) the positive slope in the [1.1–1.8]  $\mu\text{m}$  range, (ii) the shape of the 1.9  $\mu\text{m}$  band, (iii) the shape of the 2.3  $\mu\text{m}$  spectral “shoulder,” and (iv) the Fe/Mg-OH band position at 2.3  $\mu\text{m}$  are all very well reproduced. We consider the presence of vermiculite mixed with smectites very likely on Mars.

[57] In addition to the 2.3  $\mu\text{m}$  band, a smaller band is at times seen in the 2.22–2.25  $\mu\text{m}$  range as exemplified in the bottom three spectra of Figure 10a and in Figure 11. As it is very shallow and found within the left wing of the 2.3  $\mu\text{m}$  band, it is difficult to detect. We crudely estimate its presence in at least 10% of Fe/Mg phyllosilicates spectra. This band is centered at a higher wavelength than the Al-OH band present in Al-rich phyllosilicates, and these spectra consequently differ from spatial mixtures of Al and Fe/Mg clays, although such mixtures are found occasionally (e.g., blue spectrum of Figure 13). The band position is instead consistent with that of AlFe-OH and AlMg-OH structural bands found in phyllosilicates with (Al, Fe), (Al, Mg), or (Al, Fe, Mg) cations [e.g., *Bishop et al.*, 2008a]. To further investigate the origin of this additional band, we compare the CRISM spectra to pure end-members of (Al, Fe, Mg) chlorite, (Al, Fe) nontronite, and (Mg) saponite (top three spectra of Figure 11). We also build linear (spatial) mixtures of saponite with several micas, a vermiculite, an amphibole, and a chlorite. The mineral fraction is adjusted using the standard gradient-expansion curve fitting method so as to produce the best fit to the CRISM spectra. Based on these spectra, four possible origins for this band are discussed:

[58] (1) The first possibility is the presence of Fe/Mg-bearing micas (e.g., biotite, clintonite, glauconite) and/or vermiculites. Fe/Mg micas reproduce well the overall spectral shape and additional 2.22–2.25  $\mu\text{m}$  band (Figure 11). Mixed with saponite they produce very good matches to the CRISM spectra. As discussed earlier in this section, we find that the best overall match to most Fe/Mg phyllosilicates on Mars are (Al, Fe<sup>2+</sup>, Mg)

**Table 1.** Summary of all Hydrous Minerals Detected With OMEGA and CRISM to Date<sup>a</sup>

Mineral type	Group	Name	Composition	In Fig.	Lab. sp.
Phyll.	kaolins	halloysite	$\text{Al}_2\text{Si}_2\text{O}_5(\text{OH})_4$	13	RELAB
Phyll.	serpentine	lizardite	$\text{Mg}_3\text{Si}_2\text{O}_5(\text{OH})_4$	*	RELAB
Phyll.	smectite	montmorillonite	$(\text{Ca}, \text{Na})\text{Al}_2\text{Si}_4\text{O}_{10}(\text{OH})_2$	13	RELAB
Phyll.	smectite	beidellite	$(\text{Na})\text{Al}_2(\text{Si}_3, \text{Al})\text{O}_{10}(\text{OH})_2$	13	RELAB
Phyll.	smectite	nontronite	$(\text{Ca}, \text{Na})\text{Fe}_2^{3+}(\text{Si}_3\text{Al})\text{O}_{10}(\text{OH})_2$	10	RELAB
Phyll.	smectite	saponite	$(\text{Ca}, \text{Na})\text{Mg}_3(\text{Si}_3\text{Al})\text{O}_{10}(\text{OH})_2$	10	RELAB
Phyll.	mica	vermiculite	$(\text{Ca}, \text{Mg})(\text{Si}_3\text{Al})(\text{Al}, \text{Mg}, \text{Fe})_2\text{O}_{10}(\text{OH})_2$	10	RELAB
Phyll.	mica	muscovite	$(\text{K})\text{Al}_2(\text{Si}_3, \text{Al})\text{O}_{10}(\text{OH})_2$	13	USGS
Phyll.	mica	illite	$(\text{K}, \text{H}_3\text{O})(\text{Al}, \text{Mg}, \text{Fe})_2(\text{Si}_3, \text{Al})\text{O}_{10}(\text{OH})_2$	13	RELAB
Phyll.	mica	margarite	$\text{CaAl}_2(\text{Al}_2\text{Si}_2)\text{O}_{10}(\text{OH})_2$	13	USGS
Phyll.	chlorite	clinocllore	$(\text{Mg}, \text{Fe}, \text{Al})(\text{Mg}, \text{Fe}^{2+})_5(\text{Si}_3, \text{Al})\text{O}_{10}(\text{OH})_8$	11	USGS
Phyll.	prehnite	prehnite	$\text{Ca}_2\text{Al}_2\text{Si}_3\text{O}_{10}(\text{OH})_2$	◦	RELAB
Salt	sulfate	gypsum	$\text{CaSO}_4 \cdot 2(\text{H}_2\text{O})$	12	RELAB
Salt	sulfate	bassanite	$2\text{CaSO}_4 \cdot (\text{H}_2\text{O})$	12	USGS
Salt	sulfate	alunite	$\text{KAl}_3(\text{SO}_4)_2(\text{OH})_6$	12	RELAB
Salt	sulfate	amarantite?	$\text{Fe}^{3+}(\text{SO}_4)(\text{OH})$	12	♦
Salt	sulfate	jarosite	$\text{KFe}^{3+}_3(\text{SO}_4)_2(\text{OH})_6$	12	RELAB
Salt	sulfate	rozenite	$\text{Fe}^{2+}\text{SO}_4 \cdot 4(\text{H}_2\text{O})$	12	RELAB
Salt	sulfate	szomolnokite	$\text{Fe}^{2+}\text{SO}_4 \cdot (\text{H}_2\text{O})$	12	RELAB
Salt	carbonate	magnesite	$\text{MgCO}_3$	●	RELAB
Tectos.	zeolite	analcime	$\text{NaAlSi}_2\text{O}_6 \cdot (\text{H}_2\text{O})$	12	USGS
Tectos.	zeolite	gismondine	$\text{Ca}_2\text{Al}_4\text{Si}_4\text{O}_{16} \cdot 9(\text{H}_2\text{O})$	12	RELAB
Tectos.	opaline silica	opal	$\text{SiO}_2 \cdot n(\text{H}_2\text{O})$	†	RELAB
Inos.	amphibole	riebeckite	$\text{Na}_2(\text{Fe}_2^{3+}\text{Fe}^{3+})\text{Si}_8\text{O}_{22}(\text{OH})_2$	13	USGS
Soros.	epidote	epidote	$\text{Ca}_2(\text{Fe}^{3+}, \text{Al})_3(\text{SiO}_4)_3(\text{OH})$	♣	USGS

<sup>a</sup>From left to right: mineral type, mineral group, mineral name, generic chemical composition, location of the spectra in a figure of this paper or citation to another paper, source of the laboratory spectrum used to make the identification. Phyll.: phyllosilicates; Soros.: sorosilicates; Tectos.: tectosilicates; \*: *Ehlmann et al.* [2010]; ◦: *Ehlmann et al.* [2009]; ●: *Ehlmann et al.* [2008a]; ♦: *Morris et al.* [2009]; ♣: *Carter et al.* (submitted manuscript, 2012); †: *Milliken et al.* [2008].

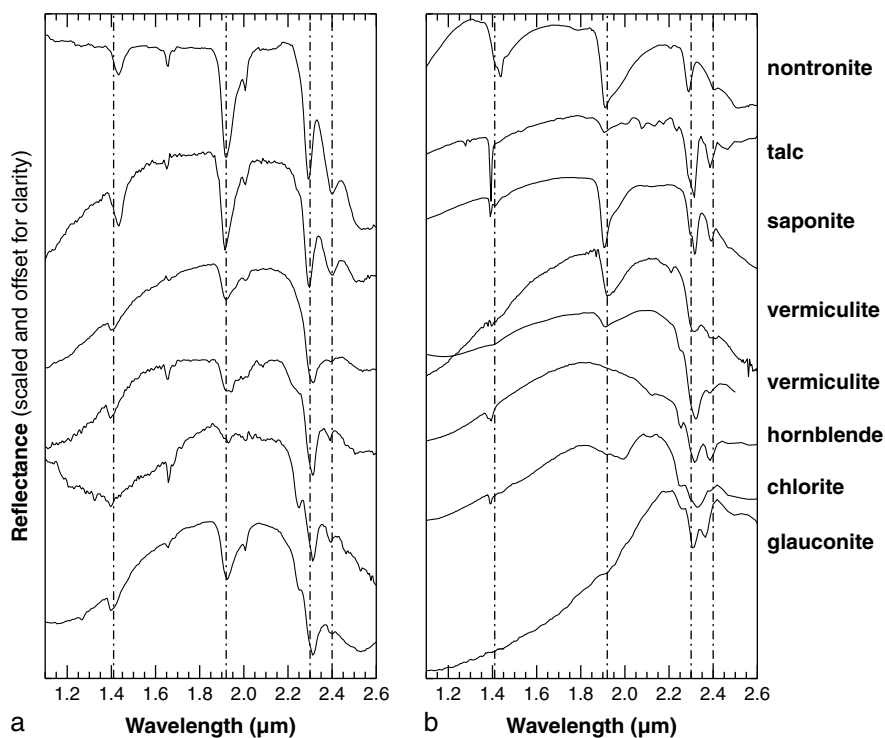


**Figure 10.** Spectral diversity of Fe/Mg phyllosilicates on Mars. (a) CRISM spectra representative of this diversity. (b) Candidate laboratory spectral matches. The listing of the identified hydrous minerals on Mars, their composition, and the source of the laboratory spectra used to identify them are summarized in Table 1.

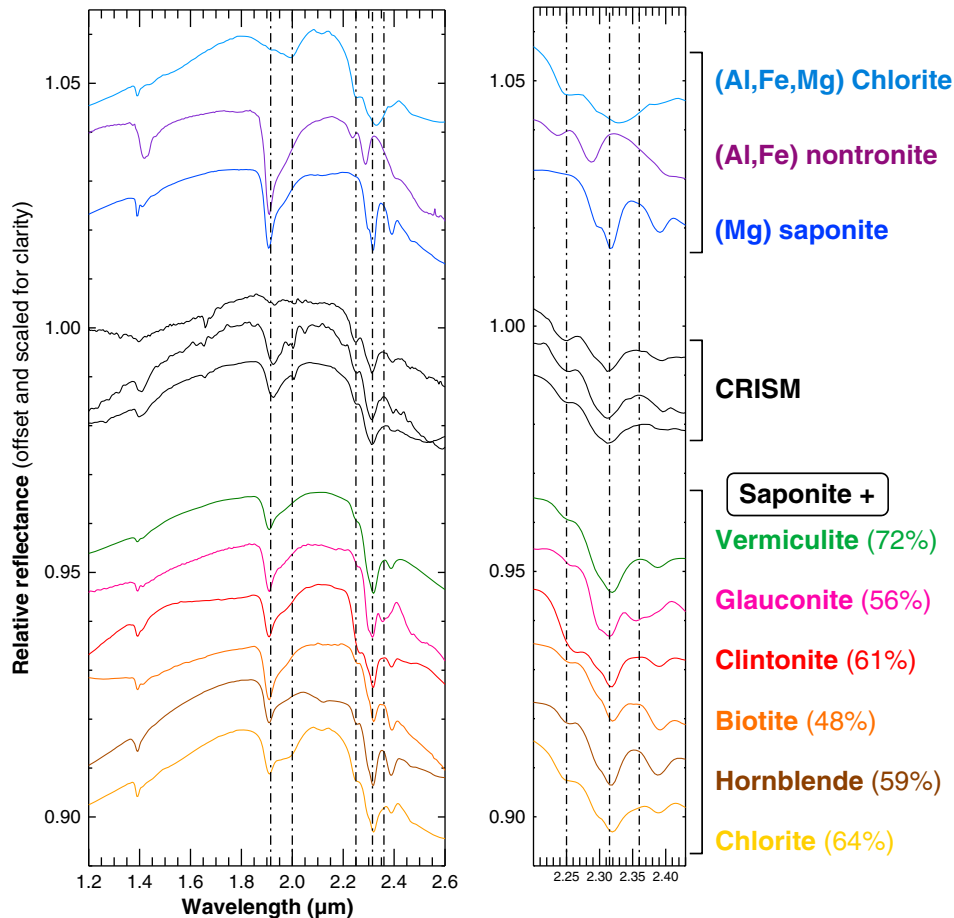


**Figure 11.** Example of Fe/Mg-phyllsilicate spectrum with additional 2.22–2.25  $\mu\text{m}$  band compared to best fit mixtures of laboratory spectra. The top three spectra are pure end-members of chlorite, nontronite, and saponite. The three example CRISM spectra are in black in the middle. The bottom six spectra are best fit linear mixtures of (Mg) saponite smectite with X% of 3 micas (glaucosite, clintonite, biotite), a vermiculite, the amphibole hornblende, and a chlorite. The right panel is a close-up on the 2.25–2.4  $\mu\text{m}$  bands.

vermiculites. Contrary to micas, vermiculite alone provides a very good fit to most Fe/Mg phyllosilicates.

[59] (2) The presence of (Al, Fe, Mg) smectites, perhaps as mixed-layered clays. Smectites with both Al and Fe or Al and Mg in their structure can induce AlFe-OH or AlMg-OH bands in the 2.22–2.25  $\mu\text{m}$  region. A spectrum of (Al, Fe) nontronite is shown in purple in Figure 11. Neither the position nor the shape of the 2.285  $\mu\text{m}$  Fe-OH band is impacted by the presence of the Al cation when compared to a pure (Fe) nontronite spectrum [Bishop *et al.*, 2008a], so we refer to Al-rich clays when the proportion of Al compared to Fe/Mg is high enough to induce Al-OH absorption bands. However, both the 2.22–2.25 and 2.85  $\mu\text{m}$  bands do not fit the CRISM spectra (black) as the sample lacks the Mg cation. Similarly to (Al, Fe) nontronite, we do not expect a change of the Mg-OH band for (Al, Mg) smectites compared to purely (Mg) smectites. As shown in Figure 11 with saponite (blue), the Mg-OH band is sharp and symmetrical and does not perfectly fit that of our spectra (black), even though the latter have the sharpest Mg-OH band found to-date (to be compared with the other CRISM spectra of Figure 10). We therefore do not consider (Al, Mg) smectites the most likely explanation.

[60] (3) Mixed-layered clays with a (Al, Fe, Mg) smectite/chlorite (corrensite) structure. The possibility for mixed-layered

clays has been proposed by several workers including Milliken *et al.* [2010] to explain our inability to provide an exact match to some spectral features of Fe/Mg phyllosilicates on Mars. Comparison with pure Fe or Mg end-member spectra (nontronite and saponite) shows a slight shift in the Fe/Mg-OH band position and shape (slightly asymmetrical and smoother on Mars than their end-member counterparts) which could be explained by the mixing of smectite layers with corrensite or chlorites. Chlorites have a 2.22–2.25  $\mu\text{m}$  band due to Al in its structure which could explain the spectra considered here. When inter-layered with smectites as corrensite, we find that the resulting spectrum has an intermediate shape between that of pure smectite (saponite) and pure chlorite. While this spectrum does exhibit this additional 2.22–2.25  $\mu\text{m}$  band, it also deforms the 2.3  $\mu\text{m}$  band which becomes a large spectral shoulder, thus incompatible with some of our observations. If we consider instead a linear mixture of two-third chlorites and one-third saponite (yellow spectrum in Figure 11), we find a good fit to the CRISM spectra in the 2.2–2.4  $\mu\text{m}$  region. While the fit is good in this region, the 1.9  $\mu\text{m}$  band of the CRISM spectra is not modified as expected by the diagnostic 2.0  $\mu\text{m}$  band in chlorites, making large amounts of mixed chlorites unlikely. However, small amounts of chlorites mixed with saponite cannot be excluded.

Signatures of chlorite not mixed with an Fe/Mg clay are often found on Mars, and they exhibit this 2.0  $\mu\text{m}$  band.

[61] (4) Another spectral combination is a mixture of Fe/Mg smectites with amphibole (e.g., hornblende). Some amphiboles such as (Al, Mg) glaucophane or (Al, Fe, Mg) hornblende have a spectrum very similar to micas and some vermiculites as they also exhibit the 2.22–2.25, 2.30, and 2.38–2.4  $\mu\text{m}$  bands. Both mineral groups are good candidates to account for the CRISM spectra. The linear mixture of saponite and hornblende (brown spectrum of Figure 11) provides an overall good match to the spectral shape in the 1.1–2.65  $\mu\text{m}$  range and of both the shapes and positions of the 2.3 and 2.22–2.25  $\mu\text{m}$  bands.

[62] Mixtures of smectites and amphiboles at such frequent occurrences would be surprising since amphiboles form metamorphically at great depth and high temperature while smectites are typically in a low temperature/shallow depth phase. Conversely, micas/vermiculites are common minerals in terrestrial basalts. Fe/Mg micas have not yet been detected on Mars but have been hypothesized in mixtures with Fe-rich smectites in Mawrth Vallis [Bishop *et al.*, 2008b; McKeown *et al.*, 2009], while K/Al micas have been detected on rare occasions. Moreover, vermiculites are a common alteration product of biotite micas on Earth. Therefore, given the available laboratory spectra and based on common mineral assemblages on Earth, we consider likely the possibility that micas variably altered to vermiculite are found mixed with smectites on Mars. In summary, we find that the vast majority of spectra are very similar but are not compatible with the spectra of pure  $\text{Fe}^{3+}$  nontronite or pure saponite smectites, and occasionally exhibit a very weak “mica band” around 2.22–2.25  $\mu\text{m}$ .

[63] In this work, we did not take into account possible environmental controls on the spectral shape and bands of Martian clays as investigated by, e.g., Gavin and Chevrier [2010], Gavin *et al.* [2011], Morris *et al.* [2011], Daly *et al.* [2011], and Che and Glotch [2012] which include desiccation, thermal heating, and mechanical shock. In the case of this possible “mica band,” laboratory work using a mineralogical proxy closer to the Martian species may provide an alternative so as to its origin.

#### 4.2.2. Serpentes and Carbonates

[64] Serpentes have two additional weak and sharp bands at  $\sim 2.12 \mu\text{m}$  (Si-O bend) and at  $\sim 2.5 \mu\text{m}$ . Fe/Mg carbonates (e.g., siderite/magnesite) also have a smooth additional  $\text{CO}_3^{2-}$  band at 2.5  $\mu\text{m}$ . Following guidelines established when both types of minerals were first reported on Mars [Ehlmann *et al.*, 2008b, 2009], all these additional bands are required to make a detection. Because the 2.12  $\mu\text{m}$  band is weak and the SNR usually too low to discriminate between a sharp and smooth 2.5  $\mu\text{m}$  band, we grouped these two minerals in the same class and only occasionally managed to discriminate between the two. Over 90 carbonates and serpentes exposures have been identified thus far, expanding the sample size by a factor of 4 to 5 compared to previous investigations [Ehlmann *et al.*, 2011a, 2011b]. These exposures are often found in close occurrence with spectrally pure olivine or olivine mixed with phyllosilicates. Some additional tens of exposures on Mars show evidence for altered olivine, but lack the additional bands to definitely identify carbonates or serpentes. Altogether, the amount of serpentine on Mars is highly limited,

arguing against a planetary-scale serpentinization as the dominant aqueous alteration process.

#### 4.2.3. Zeolites and Sulfates

[65] Zeolite spectra are dominated by a large shoulder between 2.3 and 2.4  $\mu\text{m}$ , a sharp symmetrical band at  $\sim 1.9 \mu\text{m}$  (similar or sharper than that of phyllosilicates) and a small band at  $\sim 1.4 \mu\text{m}$ . All three are due to bound water [Clark *et al.*, 1990]. Occasionally, smaller bands can be seen at  $\sim 1.2 \mu\text{m}$ , at  $\sim 1.8 \mu\text{m}$ , in the right wing of the 1.9  $\mu\text{m}$  band, at  $\sim 2.2 \mu\text{m}$ , and in the 2.3–2.4  $\mu\text{m}$  range. These are due not only to water but also to Metal-OH bends with cations Al, Fe, Ca, and Na [Cloutis *et al.*, 2002]. Hydrated sulfates, and hydrated salts in general (except for carbonates which have specific  $\text{CO}_3$  absorptions), also have their spectra dominated by water bands. Laboratory studies [e.g., Hanley *et al.*, 2011] have shown that while some spectra of salts have very specific features when dehydrated or in low hydration states, they gradually lose these diagnostic features and the spectra become very similar to that of pure water ice with an increasing hydration state. The presence of polyhydrated sulfates versus other salts on Mars has been asserted on the basis of (i) in situ measurements at Sinus Meridiani by the MER/Opportunity rover co-observed by OMEGA then CRISM. (ii) The unambiguous detection of mono/semi-hydrated sulfates (e.g., kieserite) at proximity to polyhydrated sulfate exposures. Identically to some zeolites, a few hydroxylated sulfates have Metal-OH bands that have allowed their definite identification, such as (K, Al) alunite and (K, Fe) jarosite. (iii) The nearby presence of other hydrous minerals indicating an acidic environment compatible with sulfate precipitation (e.g., kaolins, opal, (Al, Fe)-nontronite). There are however a number of exposures on Mars where these three supporting evidences are not found, and while sulfates are almost always proposed in OMEGA and CRISM studies, other types of hydrated minerals are a viable alternative in these cases.

[66] Figure 12 presents a representative sample of zeolite and sulfate/hydrated salt spectra from CRISM (left) compared to laboratory analogues (right). With the exception of (Na)-analcime (first reported in Ehlmann *et al.* [2009]), we found no other zeolite spectrum that perfectly matched the CRISM data. (Na) natrolite was reported in this previous study but we found no substantial evidence for its presence in our data set. Potential matches include (Ca)-gismondine, (Na, K, Ca) clinoptilolite, (Na, K, Ca) mordenite, and (Na, Ca) thomsonite. While the exact mineral is not identified, we see variations in the shape and position of 2.3–2.4  $\mu\text{m}$  spectral shoulder and 1.9  $\mu\text{m}$  band which indicate variable cation compositions and mineral structures. In about  $\sim 20$ –40% of the zeolite spectra, we found a very weak band at 2.2  $\mu\text{m}$  indicative of AlNa-OH transitions [Cloutis *et al.*, 2002]. This band strengthens our identification of zeolites as it is not found in polyhydrated sulfates.

[67] Excluding the few sulfates and zeolites which can be unambiguously discriminated, we find that the only way to attempt their discrimination lies in the position of the 2.3–2.4  $\mu\text{m}$  shoulder and the shape of the 1.9  $\mu\text{m}$  band. The shoulder is typically shifted toward shorter wavelengths in polyhydrated sulfates whereas the 1.9  $\mu\text{m}$  band is typically sharper and more symmetrical in zeolites. Based on these criteria, we find that the vast majority (>80%) of

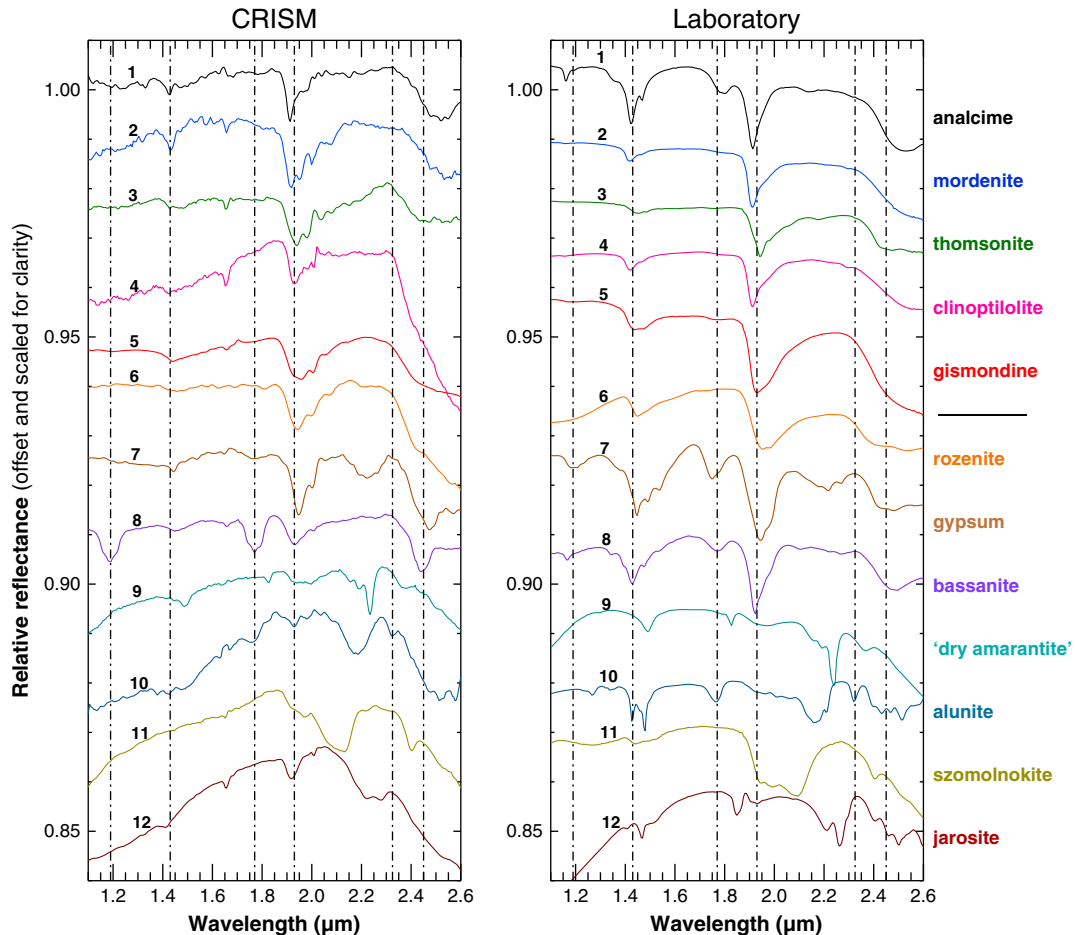


**Figure 12.** Spectral diversity of zeolites and sulfates on Mars. CRISM spectra of zeolites and sulfates on Mars (left). Each spectrum is color coded according to its best match found in spectral repositories (right).

minerals detected within the zeolite/sulfate class are likely to be zeolites.

[68] The other 20% of detections are likely to be polyhydrated sulfates. A good match is (Fe)-rozenite but many other sulfate spectra can be considered. A minority are mono/semi-hydrated sulfates (including a mineral akin to (Mg)-kieserite or (Fe)-szomolnokite and (Ca)-bassanite). These have been reported in previous works [e.g., *Gendrin et al.*, 2005; *Roach*, 2009; *Wray et al.*, 2010]. An even smaller number of exposures are consistent with the hydroxylated sulfates alunite, jarosite, and a de-hydrated ferric sulfate hydroxide with the same structural composition as amaranite. These were first reported in *Swayze et al.* [2008], *Farrand et al.* [2009], and *Massé et al.* [2008].

#### 4.2.4. Al-Smectites, Al-Kaolins, and Al-Mica

[69] Figure 13 summarizes the spectral diversity of Al-phyllsilicates on Mars. Al-smectites have been identified since the earliest detections of clays [*Bibring et al.*, 2006], and their composition is often inferred to be between that of montmorillonite and beidelite. These two minerals exhibit fine variations in the position of their diagnostic 2.2  $\mu\text{m}$  band which we also experienced in our set. We find Al-smectites and Al-kaolins to be present at about equal frequency on Mars (Figure 9).

[70] Al-kaolins are kaolinite and halloysite. They are discriminated based on their sharp doublet band at 2.17/2.21  $\mu\text{m}$ ,

a weaker doublet at 1.38/1.41  $\mu\text{m}$ , and other very small bands at 2.3 and 2.4  $\mu\text{m}$ . Kaolinite is non-hydrated and therefore should not exhibit the 1.9  $\mu\text{m}$  band, whereas halloysite does. In practice, laboratory spectra of kaolinite taken in ambient air display this 1.9  $\mu\text{m}$ , likely due to adsorbed water. This band is almost systematically found in CRISM spectra, but we do not attempt to discriminate between kaolinite and halloysite as it is very sensitive to the hydration state of the mineral.

[71] Both Al-smectites and Al-micas present a symmetrical band centered at 2.2  $\mu\text{m}$  but micas present two additional bands at  $\sim 2.35/2.43$   $\mu\text{m}$  that should allow their discrimination (Figure 13). Because this band sometimes coincides with the Fe/Mg-OH bands of Fe/Mg phyllosilicates, micas can be mistaken for mixtures of Al + Fe/Mg clays and only very high SNR spectra can allow their definite identification. Al-micas are a very rare phase on Mars and only the (Al, K) micas illite and muscovite have been reported to date [e.g., *Mustard et al.*, 2008; *Ehlmann et al.*, 2009]. We report the detection of a new (Ca, Al) mica on Mars, margarite, and the tentative detection of the (Na, Fe) amphibole riebeckite. Margarite not only exhibits common 2.2, 2.35, and 2.43  $\mu\text{m}$  bands of Al-micas but also exhibits a weak 2.26  $\mu\text{m}$  band that is found in CRISM data (purple spectrum in Figure 13). Margarite is only reported in one exposure to date (CRISM observation FRT0001188F,  $\sim [65.8^\circ\text{E}, -28^\circ\text{N}]$ ). Similarly, one exposure exhibits a signature akin to margarite but which overall spectral shape is best

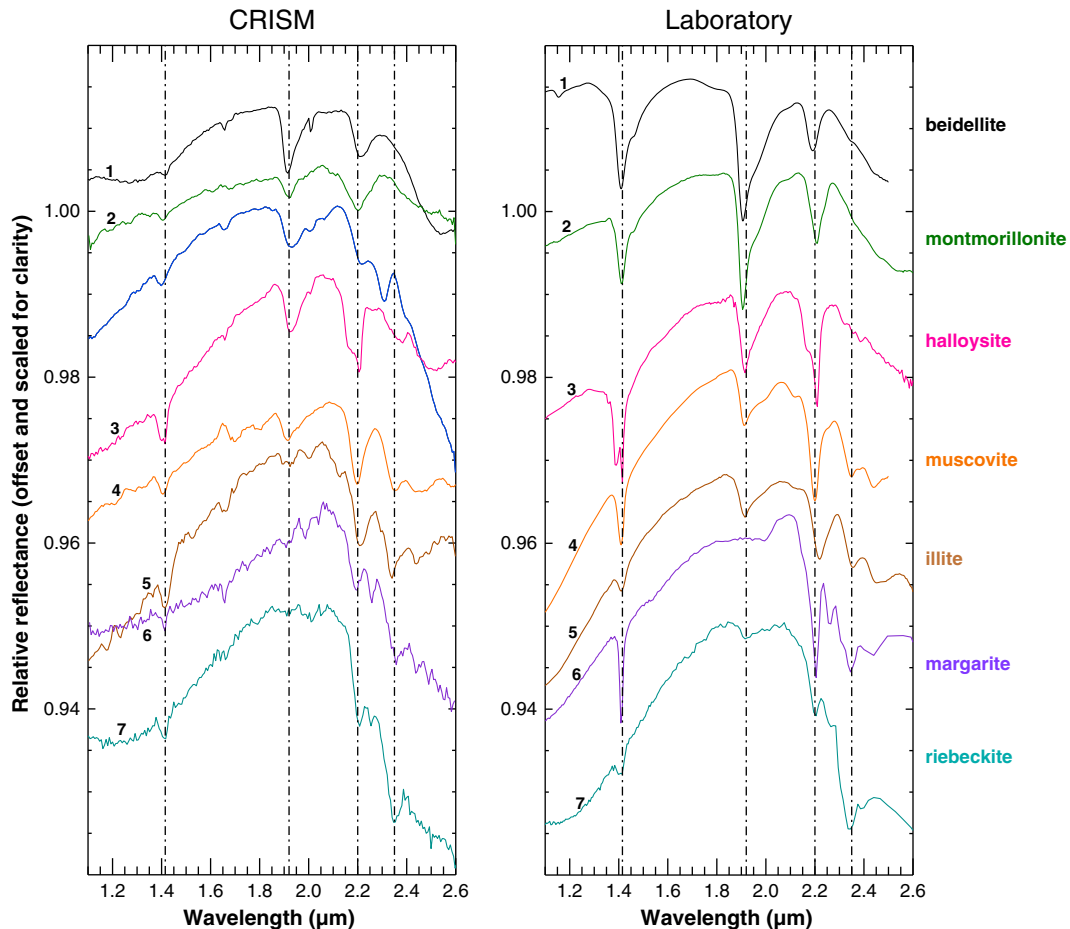


**Figure 13.** Spectral diversity of Al-rich phyllosilicates on Mars. CRISM spectra of Al smectites, kaolins, micas, and possibly amphibole (left). Each spectrum is color coded according to its best match found in spectral repositories (right). The blue spectrum of the left panel shows a mixture of Al and Fe/Mg-rich phyllosilicates seen in many CRISM observations for which no single laboratory spectrum provides a satisfactory match.

matched by riebeckite (CRISM observation FRT0000634B,  $\sim[258.8^{\circ}\text{E}, -28.8^{\circ}\text{N}]$ ). Riebeckite is not an Al-bearing amphibole but it exhibits a hydroxyl-lattice combination band that creates a feature at  $2.26\ \mu\text{m}$ .

## 5. Dating the Hydrous Mineral Exposures on Mars

[72] Because hydrous minerals place strong constraints on the surface and subsurface environments, they are key markers of the ancient surface and subsurface conditions. For example, the geothermal gradient and water availability in the crust are expected to dictate what mineral species form as a function of depth, and these evolved through time. The paleoclimate and geochemical state of the surface governed the fate of water at the surface and subsurface (temperature, salinity, pH, stability) which in turn impacted mineral formation/transformation. Hence placing time constraints on their formation provides snapshots of the evolution of the climate and geological state of Mars at various epochs.

[73] Figure 14a shows that a vast majority of hydrous minerals, primarily phyllosilicates, are found in terrains of

Noachian age. Fewer hydrous mineral exposures are found in Hesperian-aged terrains and a negligible number are found in Amazonian-aged terrains. It is possible to investigate further the age of the hydrous mineral-bearing terrains by using the global geological map of Mars from *Scott and Tanaka* [1986] which classifies the Martian surface in 54 geological units dated using crater counting. The map is largely based on low resolution imagery from Viking data has recently been upgraded by *Tanaka et al.* [2012]. We use the updated epoch boundary ages from *Hartmann* [2005]. Figure 14b shows a histogram of the hydrous mineral occurrence frequency with their unit's age, from the Early Noachian (EN) to the Late Amazonian (LA). For each hydrous mineral detection, we attribute a single geological unit age given the relative small size of the mineral exposures compared to the size of the units. Only very few terrains have been dated to within a high degree of precision ( $<10\text{--}100\ \text{Myr}$ ), and many of the hydrous mineral bearing terrains have a unit-age that can span parts or entire epochs. Since the average unit age may not reflect the true unit's age or age span, we chose to keep this temporal dimension for each unit when building the histogram of detection frequency as a function of time. For each detection is given a horizontal

dimension in the histogram which corresponds to the age span that was provided in the geological map (top panel of Figure 14b). Finally, as each unit age is not equally represented in terms of surface coverage on Mars, we normalize each data entry (horizontal bar in the histogram) by the surface coverage of each corresponding unit. The result is shown in the bottom panel of Figure 14b.

[74] Most of the detections occur inside old Noachian terrains. The occurrence frequency is much lower but remains constant in terrains dated from the middle of the

Noachian (MN) to those of the middle of the Hesperian (MH) and then slowly decays to a near-zero value in terrains dating from the late Hesperian onward.

[75] The ages shown correspond to geologic units, but do not necessary reflect the time of hydrous mineral formation. Indeed, the age of some mineral outcrops, as well as the corresponding alteration from which they formed, might not reflect that of the dated unit. Alteration can be younger than the unit, for example, in the case of younger fluid circulation or weathering. Alteration can be older than the

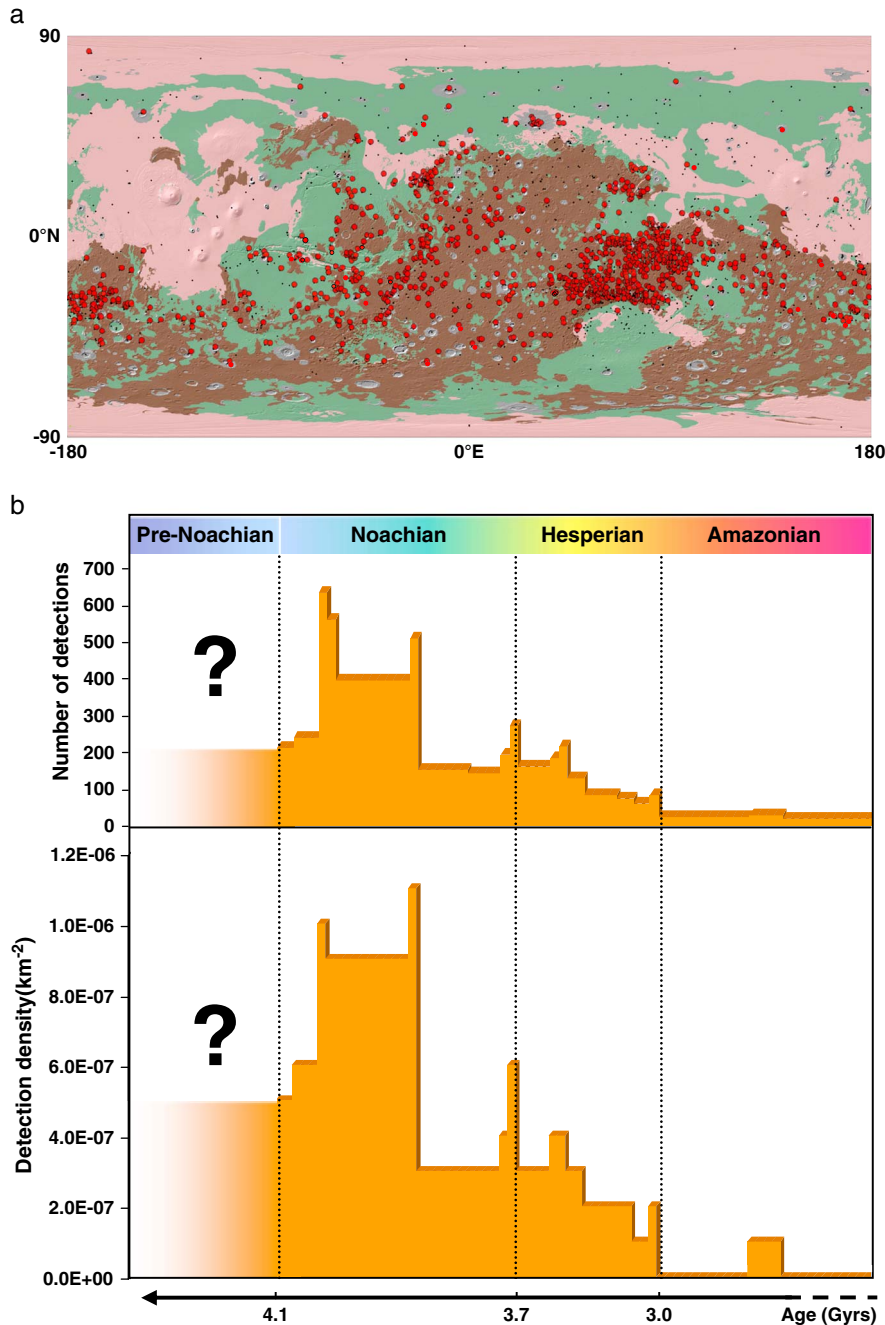


**Figure 14.** (a) Global map of hydrous minerals (red dots) according to terrain age (brown is Noachian, green is Hesperian, and pink is Amazonian) modified from *Scott and Tanaka* [1986]. Black dots show the location of CRISM observations which did not yield detections of hydrous minerals. (b) Detection frequency and surface density as a function of time.

outcrops, for example, in the case of clays transported and accumulated in sedimentary bodies. Nevertheless, the paucity of alteration signatures in Amazonian (and to a lesser extent Hesperian) terrains demonstrates a posteriori that the hydrous minerals detected in the Noachian terrains have a poor chance to date from this late period. As discussed in section 6, impact-driven hydrothermal formation of clays is likely a minor formation process although some examples have been found which mostly date to the Hesperian to Amazonian periods. Noachian-aged craters are usually too degraded in order to identify potential hydrothermal systems there (most have been infilled and/or eroded), but a study of the clay's geomorphic context does not argue in favor of massive Noachian-aged impact-driven hydrothermal clay formation. Thus, the trend observed on the histogram shows that we can use these ages as representing roughly the alteration periods, and not only the age of the corresponding units. Moreover, the crater counting technique prevents from measuring ages older than the Early Noachian (EN), essentially starting with the Hellas related impact ( $\sim 4.1$  Gyr), although some hydrated minerals (Fe/Mg phyllosilicates in particular) could well have formed earlier and have been identified in EN or younger terrains.

[76] Under the assumption that the age of the terrains in which given minerals are detected reflects that of their formation, our observations are in good agreement with an early timeline proposed by *Bibring et al.* [2006] based on which the following paradigm of Martian alteration was proposed: (i) most phyllosilicates formed during the Noachian or pre-Noachian at/near the surface and at greater depth in the crust, (ii) phyllosilicates formation dropped drastically as early as the Late Noachian and fewer hydrous minerals formed, dominated by hydrated sulfates, and (iii) the Amazonian saw very little to no aqueous alteration. This paradigm was derived based only on a few tens of detections which had been characterized so far as OMEGA's spatial resolution and coverage allowed after 2 years of investigation.

[77] The earliest period of the Noachian has a lower occurrence frequency than the rest of the Noachian. We hypothesize that this is due to two reasons: First, while units of most ages are well represented on Mars, the terrains dated to the early Noachian or earlier only cover  $\leq 4\%$  of the entire planet. Second, these oldest terrains are also the most disrupted by cratering and other resurfacing processes.

[78] The trends observed here can only be applied at a global scale and small variations of the frequency with time should not be taken into account. In particular, the discontinuities at the boundaries of periods or epochs (MN-LN, LN-EH, LH-EA) are likely due (at least partially) to a bias in the dating method of the geological units. Many units have ages which start or end at the exact same date, and the choice of this date can be somewhat arbitrary. This induces discontinuities in the form of spikes or abrupt drops in the histogram. In particular, while most phyllosilicates are found in units dated to around or before the middle of the Noachian, the abrupt drop there is likely an overestimation. Of special interest is the spike observed at the Late Noachian-Early Hesperian transition. This epoch has been proposed as an epoch of intense surface flow [*Irwin et al.*, 2005] that therefore could have induced phyllosilicate formation at the surface. Given the dating

artifacts at the boundary, we cannot conclude so as to an increased phyllosilicate formation then.

## 6. Broad Morphological Contexts

[79] The final aspect that we investigated is the morphological context. While a manual, in-depth investigation of the mineralogy was carried out for every detected exposure on Mars, it was not possible to reach the same level of detail for the morphological context. A detailed investigation of any site would require the use of various imagery data sets, thermal inertia, altimetry, geological maps, stratigraphy, etc. Such an approach is too time consuming to be applied to the entirety of the set. We therefore use a two-step process: every site is investigated using a coarse morphological/geological approach and sites of particular interest are subsequently investigated in more detail. The results of the in-depth analyses are beyond the scope of this paper and will be presented in an upcoming paper. The coarse morphological context investigation is carried out by using systematically the 100–200 m/pixel THEMIS IR daytime mosaic, 460 m/pixel MOLA topography, and the geological map mentioned above. In a few cases, THEMIS IR nighttime images were used to assess the relative thermal inertia of the altered unit. Additionally, for about half the detections (mainly CRISM-based), we used higher resolution imagery from CTX and/or HRSC and/or HiRISE.

[80] To classify major trends, we degrade the morphological context characterization level into four categories: (i) crustal outcrops, (ii) horizontal (or sub-horizontal) deposits in plains or infilling craters, many of which show layering and have been interpreted as sedimentary deposits, (iii) alluvial fans and deltas, and (iv) impact craters. These categories differ slightly from the classes used in *Murchie et al.* [2009]. Within the class “deep phyllosilicates” of *Murchie et al.* [2009], we separate those found in massifs, knobs, scarps, and mounds to those found in craters. This is done so as to prevent possible hydrothermal minerals formed following an impact to contaminate the “crustal outcrops” category. Crustal outcrops therefore will be defined as any deposit within an ancient (Noachian), indurated unit (massif, knob, within a scarp, mound) and occasional horizontal structures such as in the Mawrth Vallis region. To the exception of Mawrth Vallis, no sedimentary stratigraphy is visible in this type of context. In Mawrth Vallis, the origin of the stratified clays is still debated, but its old age and the thickness of the bulky deposit have led us to classify this deposit as crustal. The class “phyllosilicates in intra-crater fans” becomes “alluvial fans and deltas” because we find other types of hydrous minerals associated to these fluvial landforms and because these are not only found in craters. We removed the “carbonate deposits” class because carbonates are now found in various types of settings that do not broadly differ from those of other hydrous minerals on Mars. Detections of carbonates are therefore sorted into their corresponding geomorphic contexts and not given a class that would identify them by their composition instead of setting. We also ignore the polar “gypsum deposits” as they have been investigated in previous works [e.g., *Langevin et al.*, 2005; *Massé et al.*, 2010]. Because the nature of many deposits in plains remains unknown even with high-resolution imagery, we define the

“horizontal deposits” category which expands the “plains sediments” class as defined by *Murchie et al.* [2009]. It is likely that most of the exposures within the “horizontal deposits” category are in fact of sedimentary origin, although layering cannot always be seen at THEMIS spatial resolution. Classes referring to “Valles” and “Meridiani” deposits are ignored as their corresponding regions have been excluded from this study. All layered sedimentary deposits, whatever the origin were then classified as “horizontal deposits,” essentially merging the “Meridiani,” “Siliceous,” and “Valles-type” layered deposits classes. Finally, impact craters could have had an ambiguous role in the nature and distribution of hydrous minerals on Mars. They could have formed minerals in hydrothermal systems [*Abramov and Kring*, 2005] or excavated them from various depths [*Barnhart and Nimmo*, 2011]. We therefore derive a separate category for this context.

[81] Figure 15a shows the global map of hydrous minerals according to the morphological context and Figure 15b shows the context frequency. Over 50% of our detections are associated with an impact structure, i.e., a central peak/rims, wall, or ejecta. The second most common contexts are horizontal/sub-horizontal (many sedimentary) deposits and account for  $\sim 25\%$  of the detections. Crustal outcrops are found in less than 20% and alluvial fans/deltas in about 5% of cases. Because of the difficulty in precisely identifying the often degraded contexts, the limited spatial resolution of the imaging instruments and geological maps used, and some degree of arbitrary in our classification method

(as also recognized in *Murchie et al.* [2009], the occurrence frequencies presented hereafter should be considered accurate only to the several percent level.

[82] While our morphological investigation of the hydrous mineral exposures yields the same diversity as previous global surveys [*Murchie et al.*, 2009; *Ehlmann et al.*, 2011a, 2011b], we found large discrepancies on a regional scale compared with *Ehlmann et al.* [2011a, 2011b]. Instead of crustal outcrops, we map an important fraction of the northern Hellas exposures as being sedimentary plain deposits and intra-crater infilling. Some of these exposures have been identified as sediments from previous works [e.g., *Ansan et al.*, 2011; *Crown et al.*, 2010] which post-date the basin-forming event.

[83] To the exception of crustal outcrops, most of these contexts imply that the hydrous mineral exposures have been spatially remobilized since their formation. The dominance of crater structures is the best example and shows the importance of this process. While hydrothermal formation has been proposed for a few Martian craters [*Marzo et al.*, 2010; *Gross et al.*, 2012; *Mangold et al.*, 2012], we find that the majority of craters actually excavate buried hydrous minerals at various depths. This is justified by the fact that hydrothermal systems can hardly explain hydrous minerals in crater ejecta, which are a common setting within this context category as already reported in *Mangold et al.* [2007], *Mustard et al.* [2008], *Carter et al.* [2011], and *Loizeau et al.* [2012]. Although many crater

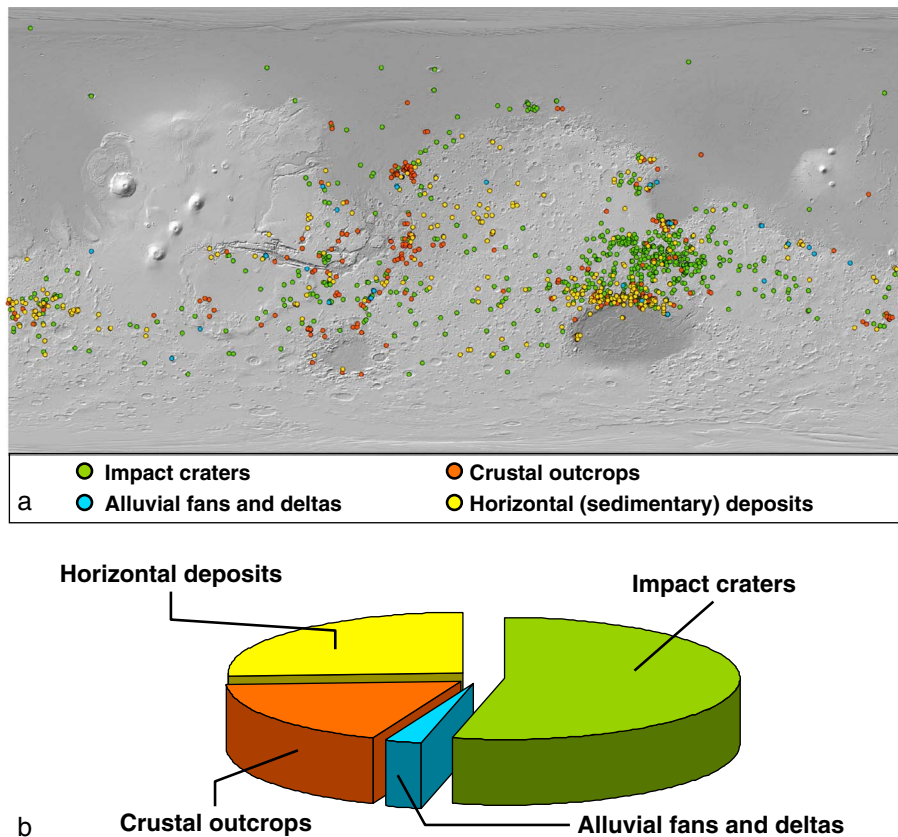


**Figure 15.** Morphological context of hydrous minerals on Mars. (a) Map of detections according to four major context categories. (b) Frequency of the hydrous mineral contexts.

hydrous exposures have a preservation state corresponding to Hesperian and Amazonian impacts [Mangold *et al.*, 2012], those having impacted Amazonian terrains seldom show any alteration, contrary to those having impacted older terrains. This demonstrates that the signal is dominated by excavation and not hydrothermal alteration, or that the latter became negligible since 3 Gyr [e.g., Mangold, 2012]. Older impacts of Noachian to Pre-Noachian ages have been mostly erased or heavily disrupted by subsequent resurfacing processes. However, impacts were more frequent at that time as a result of the formation of the Solar System and Late Heavy Bombardment and have consequently heavily gardened any clay-bearing exposure which formed then. As a result, crater excavation can be used to probe today's upper crust from the surface to several kilometers deep, but cannot be used directly to infer where nor how the excavated clays originally formed.

[84] Crustal outcrops could be the context closest to the pristine formation context. But even in this case, most original formation environments have been disturbed by >4 Gyr of gardening processes, and it is not possible to know precisely the original morphology of the surface or its stratigraphic relationship with respect to the surrounding terrains. Such inputs are required to infer the geological environments in which they formed, including whether they formed at the surface or at depth.

[85] We find that there are no strong trends in terms of composition between most morphological contexts (except when comparing impact and non-impact related contexts). The near-entire diversity of hydrous minerals is found in each context and their occurrence frequency is roughly similar. In addition, this occurrence frequency shows no clear evolution from the Noachian to the Hesperian. Collectively, these results show that interpretation of the composition of broad morphological contexts must be made very prudently, as resurfacing and remobilization processes, primarily during the Late Heavy Bombardment, have disrupted most pristine formation contexts. Only in-depth, local-scale studies may provide strong constraints on some formation environments.

[86] The impact crater context roughly differs from the other contexts in terms of composition. As shown in Figure 16, Fe/Mg clays remain the dominant phase in crater and non-crater contexts, but impact craters are relatively enriched in prehnite and chlorites. Conversely, kaolins and to a lesser extent opaline silica are less common than in the other contexts. While zeolites and sulfates are difficult to de-tangle spectrally, an in-depth spectral analysis reveals that the vast majority of strong zeolite candidates are in fact associated with impact craters while the strong sulfate candidates are not. We consider therefore that zeolites are genetically linked to craters.

## 7. Comparison With Other Data Sets

### 7.1. Fluvial Landforms

[87] Mars exhibits a number of morphological features indicative of surface and shallow sub-surface flow on early Mars. These include dendritic valley systems, sapping valleys, alluvial fans and deltas, fluvial/lacustrine sedimentary deposits and paleo-shoreline [e.g., Carr, 1996]. While many dendritic valley networks and paleolakes are found in Noachian to Early Hesperian units as are hydrous minerals, many studies have

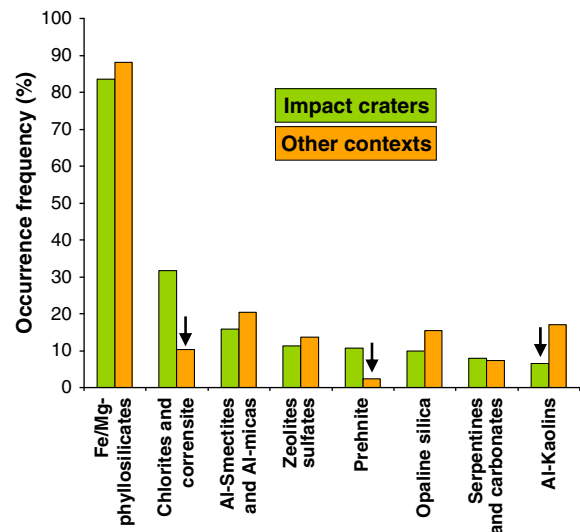


**Figure 16.** Occurrence frequency of eight spectral classes of hydrous minerals on Mars according to morphological context: impact-related (green) or non-impact related (orange). The frequency is normalized by the total number of detections in each type of context (659 and 571, respectively). The black arrows indicate strong variations (>50% difference in occurrence frequency) between the two types of contexts. Detailed spectral investigation allowed associating most zeolites with craters and sulfates with the other contexts.

put forward the low correlation between the location of altered minerals and fluvial landforms. For example, in Nili Fossae, alteration is observed regardless of the few fluvial landforms observed [Mangold *et al.*, 2007]. In Mawrth Vallis, small valleys incise a layered substratum in which the alteration pre-date valley formation [Loizeau *et al.*, 2007; 2012].

[88] Figure 17 shows the location of hydrous minerals on Mars (red) plotted over the drainage density from Hynes *et al.* [2010] and the location of putative open basin lakes from Fassett and Head [2008a]. Most of the detections occur within the low to zero drainage density regions and are uncorrelated with the open basin lakes. We also investigated the temporal correlation using the timing of events in Fassett and Head [2011]. The earliest dated period not only for dendritic valley formation (but also for all other fluvial landforms) is the middle Noachian. On the other hand, hydrous minerals predominantly formed until the middle Noachian, thus before the major observed period of valley formation. Our findings would thus favor a low degree of spatial and temporal correlations between the observed fluvial landforms and the major onset of hydrous minerals. It should be noted however that older fluvial landforms may not have been preserved by subsequent degradation processes. In addition, fluvial valleys are erosional landforms that do not provide a sink for alteration minerals—except perhaps in channel deposits but the latter are frequently buried by subsequent aeolian infilling. For example, hydrous minerals are not observed within the floor of valleys but rather exposed in their walls as the altered unit is dissected by them [e.g., Le Deit *et al.*, 2012]. The presence of valley networks particularly during the Late Noachian may however indicate a period of increased surface

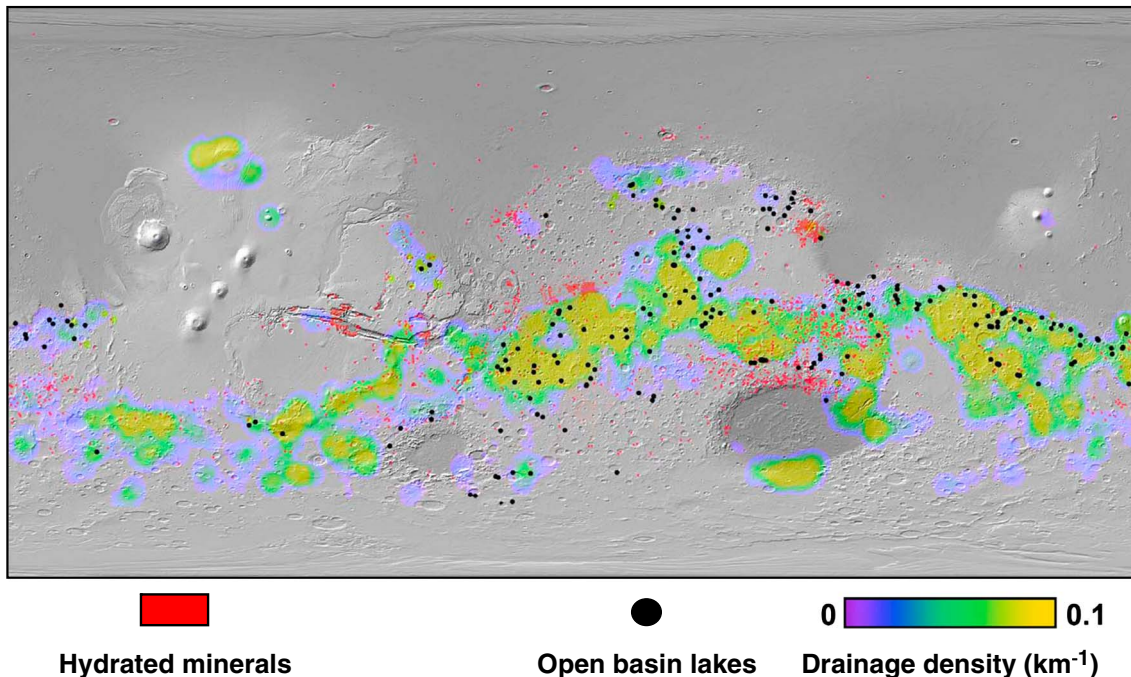


**Figure 17.** Spatial correlation between detections of hydrated minerals (red), fluvial landforms expressed as drainage density from *Hynek et al.* [2010] and putative open basin lakes (black dots) from *Fassett and Head* [2008a].

hydrological activity that may have formed surface clays or transformed pre-dating clays through leaching

[89] A closer look is required toward depositional areas such as alluvial fans and deltas. Sediment sinks and sediment transport paths have been reported in some specific locations [*Ehlmann et al.*, 2008a; *Milliken and Bish*, 2010; *Carter and Poulet*, 2012; *Goudge et al.*, 2012]. These previous findings suggest that aqueous alteration minerals identified in individual open-basin lake deposits are present as transported material as opposed to having formed in situ. We observed other examples of remobilization as alluvial fans/deltaic deposits that accumulated detrital clays formed elsewhere. Nevertheless, many of these sinks are small and late in age and also suggest a transport in a poorly altering environment as indicated by the presence of opaline silica [*Carter et al.*, 2012a]. In general, we do not find large amounts of hydrous minerals in large sedimentary sinks, but many of the latter are at low elevation and have been buried beneath subsequent volcanic plains or aeolian deposits.

## 7.2. TES- and THEMIS-Based Mineralogy

[90] The TES instrument has observed the Martian surface in the thermal range of the planet's spectrum (6–50  $\mu\text{m}$ ). The detection of hydrous silicates using TES is difficult owing to low SNR and degeneracies between hydrous and anhydrous silicate bands. Works by *Michalski et al.* [2005, 2006] have shown that clays are difficult to identify although they could account for a small fraction of the southern highlands (dark terrains). Global TES-based mineral maps (including hydrous minerals) have been derived in *Bandfield* [2002] but do not reproduce our distribution of hydrous minerals while they yield positive detections in regions that are featureless in the near-infrared (the northern lowlands in particular). However, some correlations between CRISM/OMEGA detections

of hydrous minerals and TES/THEMIS-based observations have been found locally at the outcome of detailed investigations. One example is a careful comparison of TES data with OMEGA observations of hydrous minerals that was carried out in Nili Fossae and Mawrth Vallis, for which some correlations were found indicating that some exposures can be detected in the thermal infrared [*Michalski et al.*, 2010].

[91] The TES and THEMIS also identified numerous exposures of high-silica material which could not be unambiguously identified, but for which an opal or zeolite type composition was proposed [*Michalski et al.*, 2005]. More recently, *Bandfield* [2008] identified a large exposure of high-silica bearing deposits located on the western margin of Hellas Planitia and interpreted it as having a fluvial origin. Opal or zeolites were proposed for this deposit, although phyllosilicates were also considered. We achieved an independent detection of this extended (>6000 km<sup>2</sup>) high-silica deposit in Hellas Planitia [*Carter et al.*, 2009] using OMEGA then CRISM observations. The mineral maps from OMEGA and TES are remarkably well correlated as shown in Figure 18. The mineralogy of this deposit is confirmed to be primarily opal-rich with indications of an additional zeolite component. This co-detection indicates that these data sets can be used jointly to identify zeolites and opaline on Mars.

## 8. Discussion

### 8.1. Timing of the Alteration

[92] Hydrous minerals are found in terrains that are dated from the Early Noachian to the Amazonian epochs, and their occurrence frequency has evolved with time. From section 5, a decrease in clay occurrence is observed from the middle Noachian onward, with negligible occurrences reached

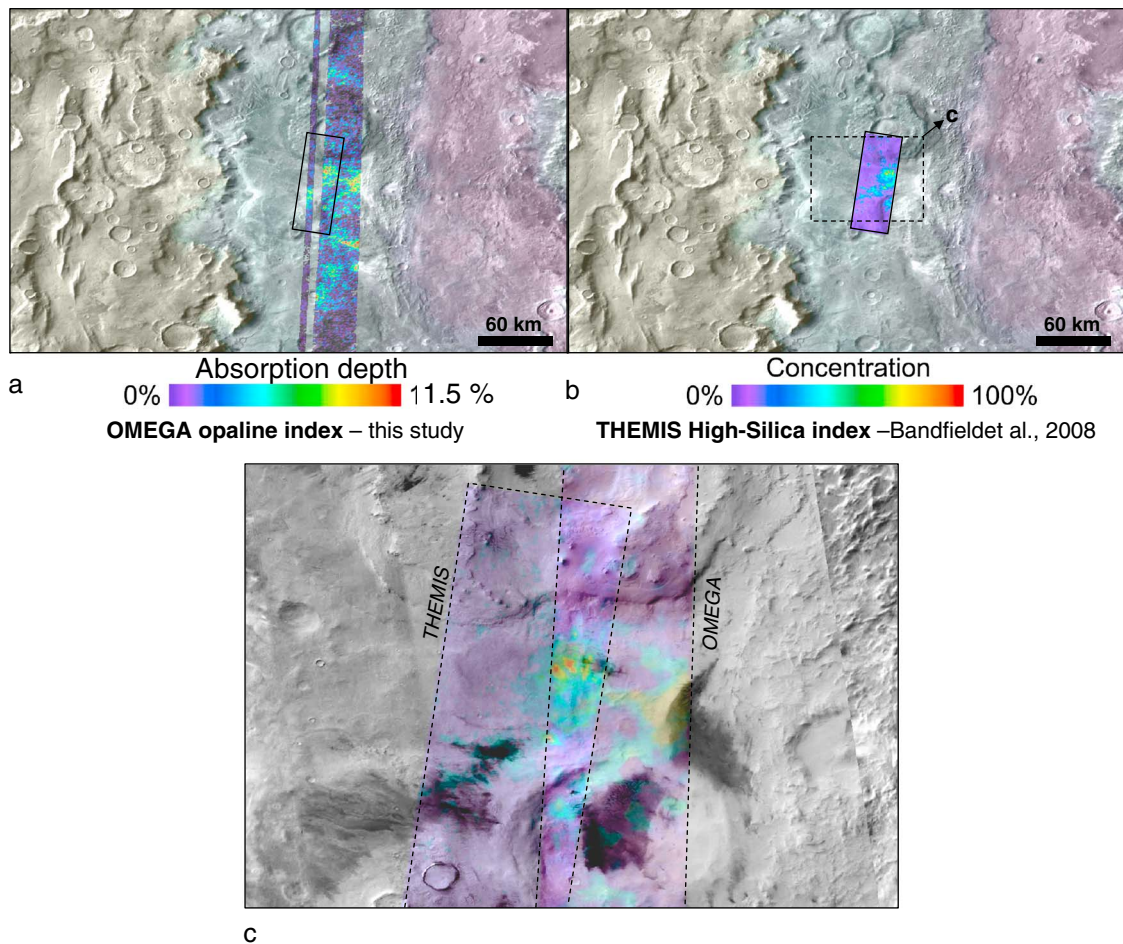


**Figure 18.** Co-detection of opaline silica and zeolites in the western margin of Hellas Planitia. (a) OMEGA mineral maps of opaline silica ( $2.25\ \mu\text{m}$  absorption band depth). The footprint of the THEMIS observation is over-plotted. (b) High-silica concentration from *Bandfield* [2008]. (c) Close-up on overlapping OMEGA and TES observations. Backgrounds are THEMIS IR mosaic with MOLA colored elevation.

around the Late Hesperian. This evolution with time is however partially biased by impact cratering. Excavation by impacts is the dominant setting of hydrous minerals on Mars, but most craters where hydrous mineral exposures are detected correspond to well-preserved craters of possible Hesperian to Amazonian ages in Noachian terrains. Thus, it could safely be inferred that most of the associated minerals are Noachian in age, or older. If Hesperian and Amazonian impacts are the dominant process to place hydrous minerals on the surface, older impacts (contemporaneous to the principal observable era of hydrous mineral occurrence) also surely played a similar role, but most such craters are too degraded (or have been destroyed completely) to allow connecting the mineral exposures to the impact structures.

[93] The global evolution with time of the mineral occurrence is also biased by the impact flux. Although the initial and Late Heavy Bombardment impacts fluxes are not well known and neither are their timings, they were orders of magnitude higher than the Hesperian and Amazonian impact fluxes. Thus, this high occurrence frequency of hydrous minerals during the first half of the Noachian may partially reflect this higher impact flux, excavating or hydrothermally forming large amounts of hydrous minerals

at great depth or at the surface. Because any terrain older than 4.1 Gyr has reached crater saturation and those slightly younger (Early Noachian) are the most resurfaced by subsequent processes, the mineral occurrence cannot be accurately inferred for the Early to Pre-Noachian epochs. Only in situ investigations and dating of clay exposures may provide answers about the state of alteration during the Pre-Noachian. In some cases, the same set of events may have produced together the set of phyllosilicates from Fe/Mg-rich species to higher leached (Al-rich) ones, but the leaching likely occurred after Fe/Mg phyllosilicate formed in many cases.

## 8.2. Formation at Non-Ambient Terrestrial Temperatures: Diagenetic, Metamorphic, and Hydrothermal Minerals

[94] On Earth, the hydrous mineralogy is mostly governed by water availability and temperature. Let us assume a simple model of the crust where temperature rises with depth due only to the geothermal gradient and porosity decreases as pressure increases. In such a case, high temperature and low W:R minerals will form at depth, while low temperature minerals will form near or at the surface, with a W:R varying depending on the presence or not of a shallow cryosphere or

hydrosphere. Metamorphic and diagenetic minerals (e.g., chlorites, prehnite, the zeolites analcime) would hence form at depth, while smectite clays (in particular Al-rich smectites and kaolins if the W:R is high) would form near or at the surface. This simple model can be applied to Mars but perturbations exist, including the possibility for deep hydrothermal Fe/Mg clay formation in heated aquifers as proposed in *Ehlmann et al.* [2011a, 2011b]. In addition, shallow hydrothermal systems (impact or volcanism related) or surface acidolysis may also perturb this trend. Global trends can nonetheless be inferred based on our statistical sample and the geomorphic setting of specific minerals.

[95] The detection of hundreds of exposures of prehnite, chlorite, and the zeolite analcime in the central peaks and ejecta of craters collectively point toward formation at kilometer depth (up to several kilometers) within the crust as also proposed by *Ehlmann et al.* [2011a, 2011b]. Prehnite is not expected to form at the surface in the presence of CO<sub>2</sub> in the atmosphere [*Frey and Robinson, 1998; Ehlmann et al., 2009*], thus excluding the possibility of impact-driven hydrothermal formation of prehnite at the surface. In *Carter et al.* [2011], the composition of the upper crust is assessed by studying the dominant hydrous minerals within the ejecta of craters excavating at depths ranging from the surface to several kilometers deep. It is found that smaller craters ( $D < 5$  km) dominantly excavate Fe/Mg-rich clays, whereas larger craters ( $D > 5$ –20 km) dominantly excavate chlorites. This result suggests a vertical transition from Fe/Mg clays to chlorites as a function of depth in the southern highlands. Figure 16 also shows that the hydrous mineralogy in crater-related contexts has a surplus of high-temperature phases compared to other contexts. This argues in favor of a gradual transition in the hydrous mineral composition within the first hundreds of meters to kilometers of the crust. These high-temperature minerals (including chlorites) could have formed by deep hydrothermal circulation of fluids or by burial diagenesis/metamorphism.

[96] In addition to formation at depth, there is compelling evidence for limited hydrothermal formation of hydrous minerals at or close to the surface. Impact-generated hydrothermal systems capable of forming hydrous minerals [e.g., *Schwenzer and Kring, 2009*] have been proposed on Mars, in Toro and Majuro craters [*Marzo et al., 2010; Mangold et al., 2012*]. The Nili Fossae serpentine-carbonate assemblages are also interpreted as resulting from hydrothermal systems [*Ehlmann et al., 2009*]. The recent detection of epidote in volcanic units of Mars (*Carter et al.*, submitted manuscript, 2012) indicates higher-temperature hydrothermal formation ( $T > 200$ –400°). Localized opaline silica and bassanite exposures were identified in relationships with volcanic centers, respectively, in Nili Patera [*Skok et al., 2010*] and Noctis Labyrinthus [*Mangold et al., 2010; Thollot et al., 2012*].

### 8.3. Formation at Ambient Temperature on the Surface: Pedogenic, Detrital, and Authigenic Clays

[97] A major unsettled question regarding early Mars is whether climatic conditions allowed surface liquid water to exist on geological timescales or instead transiently, as a result of a temporary external forcing function (e.g., obliquity change, basin-forming impact event, major volcanic outgassing event). The case for a warm and wet Noachian Mars is

challenged by the paucity and immaturity of dendritic valley networks [*Irwin et al., 2005*], the failure of some climatic models to predict an atmosphere warm and dense enough to sustain liquid water [e.g., *Gaidos and Marion, 2003; Colaprete and Toon, 2003*], and investigations of the aqueous mineralogy of Mars [*Ehlmann et al., 2011a, 2011b*]. The latter propose dominant clay formation in the sub-surface with localized, transient pockets of alteration on the surface. Here we present a set of arguments suggesting that Mars experienced periods of surface alteration capable of forming/transforming clays and other hydrous minerals at the surface.

#### 8.3.1. Fluvial Features and Sedimentary Basins

[98] Most observed fluvial landforms are dated from the middle Noachian to the early Hesperian [*Fassett and Head, 2011*], with a possible brief period of more intense runoff at the Noachian-Hesperian boundary [*Irwin et al., 2005*]. Peak clay formation occurred before, around, or until the middle Noachian. This poor correlation has been put forward as evidence that most clays formed in the sub-surface during the Noachian, but the issue of preservation limits our knowledge of fluvial landforms previous to the oldest observed. Indeed, the terrains of Early Noachian age account for under 4% of the surface, and no fluvial landforms are found in them, presumably owing to resurfacing processes. Terrains dissected by fluvial features only account for 2.2% in terrains older than the Late Noachian, and all of these are heavily degraded [*Tanaka et al., 1988*]. Thus, from the study of the clay contexts in section 6, we see that the majority of clays and the near-entirety of the oldest clays do not preserve their original formation contexts. As a consequence, the presence of a surface hydrological system (precipitation zones, runoff in valley networks, ponding in lakes) in which clays formed were transported and accumulated earlier than the Late Noachian cannot be proved nor disproved with the available data. In a hydrological system, clays concentrate in topographic lows, as such they likely have a fair chance of partially surviving impact gardening, albeit not in their original contexts. On the other hand, small dendritic valleys are easily disrupted and filled by impact gardening and other processes. Noachian clays should have accumulated in the depositional sinks of the time. These structures have however also been depositional sinks for the past 4 Gyr, accumulating thick layers of mass-wasting material, volcanic, and aeolian deposits, burying putative detrital clays at great depth [*Tanaka and Leonard, 1995; Tanaka et al., 2003*]. These basins are also some of the least favorable regions for remote-sensing observations, which can explain the paucity of detections there. In conclusion, the poor degree of correlation between hydrous minerals and observable fluvial features on Mars cannot be used as an argument to dismiss or favor significant surface clay formation.

#### 8.3.2. Phyllosilicate Composition

[99] Phyllosilicates (smectites and vermiculites in particular) are mostly surface and shallow sub-surface clay minerals which form at low temperatures (typically  $< 100^\circ\text{C}$ ) [*Velde, 2010*], at various W:R but which require long-lasting liquid water for their formation. The dominant hydrous phases on Mars are a type of Fe/Mg-rich phyllosilicate, which typically forms on Earth at rather low W:R. As discussed in section 4.2, most Fe/Mg phyllosilicate spectra on Mars are similar but are not perfectly matched by the Fe and Mg smectites end-members nontronite and saponite. A mixture of both

smectites with ferrous micas and smectites with micas altered to vermiculite is likely in most cases as they can account for the asymmetry of the 2.3  $\mu\text{m}$  band and the occasional weak 2.25  $\mu\text{m}$  band. Vermiculitization of micas is mostly a surface-weathering process on Earth. Of particular interest are aluminous clays (especially kaolins) which, in the case of a basaltic parent rock, typically form at higher W:R and/or lower pH than Fe/Mg-rich clays. They are most commonly surface-alteration minerals. Al-rich clays have often been considered to be a somewhat rare phase on Mars. *Mustard et al.* [2008] only found small amounts of kaolins while Al-phyllosilicates were restricted to a few regions of Mars (mostly in the vicinity of Mawrth Vallis). More recent work by *Ehlmann et al.* [2011a, 2011b] found an occurrence frequency of around 11%, also concentrated in select regions of Mars. In contrast we find that about one third of the hydrous exposures detected on Mars to date display Al-rich clays, with kaolins and smectites in about equal amounts while micas are a minority. The main reason for this increase in Al-clay occurrence is the use of new processing and mineral identification tools which are more sensitive to Al-clay exposures which have typically weaker signatures and smaller-sized exposures than Fe/Mg clays (by about one order of magnitude).

[100] A few investigations have found that in selected areas of Mars, Al-clays stratigraphically overlie thicker sequences of Fe/Mg clays [e.g., *Loizeau et al.*, 2010; *Noe Dobrea et al.*, 2010]. The best example is the Mawrth Vallis region where such exposures are common. Such vertical sequences are common on Earth and indicate surface weathering under non-arid climatic conditions [e.g., *Velde*, 2010; *Gaudin et al.*, 2011]. On Mars, these have also been interpreted as remnants of pockets of surface weathering and have been dated to be mostly of late Noachian age. Additional exposures of weathering sequences have also been found recently in the Thaumasia Planum region [*Le Deit et al.*, 2012]. Here, we find that these sequences are more widespread than previously found, with several additional exposures found scattered over the southern ancient highlands. While such sequences were not always formally identified, we find that the majority of Al-clays on Mars are not isolated but spatially connected (at the CRISM spatial resolution) to Fe/Mg-clays. Whenever the topography allows inferring their relative positions, we find the Al-clays to overlie the Fe/Mg clays, suggesting the presence of hundreds of additional spots exhibiting such a weathering sequence. If these widespread Al-clays indeed formed on the surface, then widespread interaction between liquid water and the basaltic crust, possibly already altered as Fe/Mg phyllosilicates, occurred on the surface, although a significant fraction of clays could still have formed at depth. The widespread occurrence of Al-clays on Mars and the presence of numerous weathering sequences are however difficult to explain if considering deep hydrothermal circulation as the main clay formation pathway as proposed in *Ehlmann et al.* [2011a, 2011b].

[101] The amount of Al-clay visible today must be considered a lower limit. Weathering sequences under non-tropical humid climates form in less volume Al clays than Fe/Mg clays [*Allen*, 2009]. As a proxy for Mars, *Gaudin et al.* [2011] describe an ancient weathering sequence on Earth where the Al clay layer accounts for the top 10 m of the sequence compared to at least 30 m of underlying Fe/Mg clays. Taking the lower estimate for erosion rates during the Noachian of  $10^{-7}$  m/yr

[*Golombek and Bridges*, 2000 and references therein], and despite a decrease during the Hesperian and Amazonian, on average several meters to tens of meters of the upper surface have been removed. Additionally, inserting these clay thicknesses into the modeling work of impact ejecta by *Barnhart and Nimmo* [2011] shows that the mixing ratio of Al-clays is roughly three times smaller than that of Fe/Mg clays. These two processes and other resurfacing processes result in a much lower survivability and detectability of Al-clays on Mars compared to Fe/Mg-clays: The Al-clay layer was preferentially disrupted and mixed with other minerals. Consequently, the  $\sim 30\%$  frequency of Al-clays (under the surface weathering scenario) is likely a lower limit.

### 8.3.3. Hydrated Salts and Opaline Silica

[102] The presence of salts (sulfates, carbonates and chlorides) is another indication that some minerals could have precipitated on the surface of Mars. Opaline silica is another mineral type which can be linked to surface alteration. First identified in Valles Marineris and Gusev crater [*Milliken et al.*, 2008; *Squyres*, 2008], these deposits were interpreted as low-temperature, low W:R, acidic alteration products. We also detect numerous opaline silica deposits on Mars, including in most deltas and alluvial fans [*Carter et al.*, 2012b] which we interpret as being in situ surface formation during or shortly following aqueous flows. These are mostly dated to the Hesperian to Amazonian periods. The authigenic opaline silica trace very arid environments usually incompatible with clay formation [*Tosca and Knoll*, 2009], thus disconnected from the major clay forming period, but still involves surface or near-surface liquid water.

## 9. Conclusion

[103] We have conducted a global-scale survey of the hydrous mineralogy of Mars based on near-infrared data from the CRISM and OMEGA imaging spectrometers. By building a large sample of over a thousand detections, we infer a number of global trends regarding the aqueous alteration on early Mars. The main results of this study are as follows:

[104] (1) Hydrous minerals are widespread on Mars. Hydrous silicates are concentrated in the southern highlands where they cover today roughly 3% of the surface.

[105] (2) Hydrous minerals are also found in the northern lowlands of Mars, in various geological units of various ages and exhibit compositional diversity. Clays have been found in old northern plain terrains and as excavated material in impact craters which originated from the basal unit formed prior to the infilling. The suite of minerals found there is similar to that of craters within the southern highlands. The ancient alteration has affected Mars at a planetary scale. Additionally, younger terrains are not devoid of alteration signatures, as evidenced by the presence of young hydrated silicates/zeolites presumably formed from volcano-ice interaction. Collectively these detections hint toward an aqueous alteration on Mars which is both widespread and spanned geological eons.

[106] (3) Most families of hydrous minerals which exist on Earth have been found on Mars, namely smectites, micas, vermiculites, kaolins, chlorites, hydrated salts, high-temperature hydroxides, hydrated silica, serpentines, carbonates, and possibly amphiboles. The most common hydrous minerals on Mars are Fe/Mg and Al-rich phyllosilicates, which many of the latter may have formed later than Fe/Mg phyllosilicates.

[107] (4) Most hydrous minerals formed on Mars before the middle of the Noachian, while some limited alteration took place later, well into the Hesperian and Early Amazonian. Degradation of the original formation context and remobilization has removed the possibility to accurately date most if not all hydrous mineral exposures.

[108] (5) The diversity of morphological contexts, albeit heavily degraded, indicates diverse formation or transformation environments. The dominant contexts are the central peaks and ejecta of impact craters, indicating massive excavation of buried hydrous minerals, which may have originally formed at depth or at/near the surface.

[109] (6) Current methods of investigation do not allow inferring the state of alteration on Mars before 4.1 Gyr nor can it accurately predict variations of the alteration environments on small temporal scales.

[110] By coupling the mineralogy to the morphology, it is possible to infer some formation or transformation environments. We find that most of the geological settings of clays and salts on Earth are also observed on Mars:

[111] (1) Formation through surface weathering, as indicated by the Al-smectite/Fe-Mg-smectite profile,

[112] (2) Detritic deposition and authigenic formation in fluvial-lacustrine and evaporitic environments,

[113] (3) Hydrothermal alteration, either impact related through volcanic activity or geothermal heating of deep aquifers,

[114] (4) Burial diagenesis of sediments and low-to-medium grade metamorphism at kilometer depth.

[115] Because of the highly degraded state of the morphological contexts on Mars, it is difficult to determine if these alteration environments were spatially and temporally connected. A prospective paper will explore these relationships further. This global-scale study shows however that these alteration environments were widespread and existed early in the history of the planet (>4 Gyr) and occurred for several hundreds of Myr, although clay formation gradually declined after the middle of the Noachian. While a large fraction of clays may have formed subterraneously, the high frequency of Al-clays observed today, likely underestimated due to resurfacing processes, also points to a strong surface component in the alteration environments on early Mars which challenges scenarios in which climatic conditions never allowed widespread clay formation on the surface within a hydrological cycle.

[116] **Acknowledgments.** We would like to thank Jack Mustard and Patricia Gavin for their very thorough review of our work and for the numerous insightful comments and corrections they provided which greatly improved the manuscript.

## References

- Abramov, O., and D. A. Kring (2005), Impact-induced hydrothermal activity on early Mars, *J. Geophys. Res.*, *110*, E12S09, doi:10.1029/2005JE002453.
- Allen, C. C. (1979), Volcano-ice interactions on Mars, *J. Geophys. Res.*, *84*, 8048–8059, doi:10.1029/JB084iB14p08048.
- Ansan, V., et al. (2011), Stratigraphy, mineralogy, and origin of layered deposits inside Terby crater, Mars, *Icarus*, *211*, 273–304, doi:10.1016/j.icarus.2010.09.011.
- Arvidson, R. E., F. Poulet, J. -P. Bibring, M. Wolff, A. Gendrin, R. V. Morris, J. J. Freeman, Y. Langevin, N. Mangold, and G. Bellucci (2005), Spectral reflectance and morphologic correlations in eastern Terra Meridiani, Mars, *Science*, *307*, 1591–1594, doi:10.1126/science.1109509.
- Balan, E., A. M. Saitta, F. Mauri, C. Lemaire, and F. Guyot (2002), First-principles calculation of the infrared spectrum of lizardite, *Am. Mineral.*,

- 870*(10), 12861290, URL <http://ammin.geoscienceworld.org/cgi/content/abstract/87/10/1286>
- Baldrige, A., S. Hook, C. Grove, and G. Rivera (2009), The ASTER spectral library version 2.0, *Remote Sens. Environ.*, *113*, 711–715.
- Bandfield, J. L. (2002), Global mineral distributions on Mars, *J. Geophys. Res.*, *107*, 5042, doi:10.1029/2001JE001510.
- Bandfield, J. L. (2008), High-silica deposits of an aqueous origin in western Hellas Basin, Mars, *Geophys. Res. Lett.*, *35*:L12205, doi:10.1029/2008GL033807.
- Baratoux, D., P. Pinet, A. Gendrin, L. Kanner, J. Mustard, Y. Daydou, J. Vaucher, and J. -P. Bibring (2007), Mineralogical structure of the subsurface of Syrtis Major from OMEGA observations of lobate ejecta blankets, *J. Geophys. Res.*, *112*, E08S05, doi:10.1029/2007JE002890.
- Barnhart, C. J., and F. Nimmo (2011), Role of impact excavation in distributing clays over Noachian surfaces, *J. Geophys. Res.*, *116*, E01009, doi:10.1029/2010JE003629.
- Bibring, J. -P., et al. (2004), OMEGA: Observatoire pour la Minéralogie, l'Eau, les Glaces et l'Activité, in *Mars Express: The Scientific Payload*, edited by A. Wilson and A. Chicarro, 37–49, pp., volume 1240 of *ESA Special Publication*, August, Noordwijk, The Netherlands.
- Bibring, J. -P., Y. Langevin, J. F. Mustard, F. Poulet, R. Arvidson, A. Gendrin, B. Gondet, N. Mangold, P. Pinet, and F. Forget (2006), Global mineralogical and aqueous mars history derived from OMEGA/Mars Express data, *Science*, *312*, 400–404, doi:10.1126/science.1122659.
- Bishop, J., J. Madejova, P. Komadel, and H. Froschl (2002), The influence of structural Fe, Al and Mg on the infrared OH bands in spectra of dioctahedral smectites, *Clay Miner.*, *370*(4), 607–616, doi:10.1180/000985502374006.
- Bishop, J., M. D. Lane, M. D. Dyar, and A. J. Brown (2008a), Reflectance and emission spectroscopy study of four groups of phyllosilicates: Smectites, kaolinite-serpentine, chlorites and micas, *Clay Miner.*, *430* (1), 35–54, doi:10.1180/claymin.2008.043.1.03.
- Bishop, J. L., et al. (2008b), Phyllosilicate diversity and past aqueous activity revealed at Mawrth Vallis, Mars, *Science*, *321*, 830, doi:10.1126/science.1159699.
- Carr, M. H. (1996), *Water on Mars*, Oxford University Press, Cary, North Carolina.
- Carter, J., and F. Poulet (2012), Orbital identification of clays and carbonates in Gusev crater, *Icarus*, *219*, 250–253, doi: 10.1016/j.icarus.2012.02.024.
- Carter, J., F. Poulet, J. -P. Bibring, S. L. Murchie, Y. Langevin, J. F. Mustard, and B. Gondet (2009), Phyllosilicates and other hydrated minerals on Mars: 1. Global distribution as seen by MEX/OMEGA. In *Lunar and Planetary Institute Science Conference Abstracts*, volume 40 of *Lunar and Planetary Institute Science Conference Abstracts*, page 2028, March.
- Carter, J., F. Poulet, J. -P. Bibring, and S. Murchie (2010), Detection of hydrated silicates in crustal outcrops in the northern plains of Mars, *Science*, *328*, 1682, doi:10.1126/science.1189013.
- Carter, J., F. Poulet, A. Ody, J. -P. Bibring, and S. Murchie (2011), Global distribution, composition and setting of hydrous minerals on Mars: A reappraisal. In *Lunar and Planetary Institute Science Conference Abstracts*, volume 42 of *Lunar and Planetary Institute Science Conference Abstracts*, p. 2593, March.
- Carter, J., F. Poulet, N. Mangold, V. Ansan, E. Dehouck, J. -P. Bibring, and S. Murchie (2012a), Composition of deltas and alluvial fans on Mars. In *Lunar and Planetary Institute Science Conference Abstracts*, volume 43 of *Lunar and Planetary Inst. Technical Report*, page 1978, March.
- Carter, J., F. Poulet, N. Mangold, V. Ansan, E. Dehouck, J. -P. Bibring, and S. Murchie (2012b), Composition of deltas and alluvial fans on Mars. In *Lunar and Planetary Institute Science Conference Abstracts*, volume 43 of *Lunar and Planetary Institute Science Conference Abstracts*, page 1978, March.
- Carter, J., F. Poulet, S. Murchie, and J. -P. Bibring (2012), Automated processing of planetary hyperspectral datasets for the extraction of weak mineral signatures and applications to CRISM observations of hydrated silicates on Mars, *Planet. Space Sci.*, doi:10.1016/j.pss.2012.11.007, in press.
- Che, C., and T. D. Glotch (2012), characterizing dehydrated and dehydroxylated phyllosilicates on Mars using thermal and near IR spectroscopy. In *Lunar and Planetary Institute Science Conference Abstracts*, volume 43 of *Lunar and Planetary Institute Science Conference Abstracts*, page 1377, March.
- Clark, R. N. (2007), USGS digital spectral library splib06a: U.S. Geological Survey, Digital Data Series 231, <http://speclab.cr.usgs.gov/spectral.lib06>
- Clark, R. N., T. V. V. King, M. Klejwa, G. A. Swayze, and N. Vergo (1990), High spectral resolution reflectance spectroscopy of minerals, *J. Geophys. Res.*, *95*, 12653–12680, doi:10.1029/JB095iB08p12653.
- Cloutis, E. A., P. M. Asher, and S. A. Mertzman (2002), Spectral reflectance properties of zeolites and remote sensing implications, *J. Geophys. Res.*, *107*, 5067, doi:10.1029/2000JE001467.

- Cloutis, E. A., et al. (2006), Detection and discrimination of sulfate minerals using reflectance spectroscopy, *Icarus*, 184, 121–157, doi:10.1016/j.icarus.2006.04.003.
- Colaprete, A., and O. B. Toon (2003), Carbon dioxide clouds in an early dense Martian atmosphere, *J. Geophys. Res.*, 108, 5025, doi:10.1029/2002JE001967.
- Crown, D. A., L. F. Bleamaster, S. C. Mest, J. F. Mustard, and M. Vincendon (2010), Geologic mapping of the NW rim of Hellas Basin, Mars: Evidence for an ancient buried landscape. In *Lunar and Planetary Institute Science Conference Abstracts*, volume 41 of *Lunar and Planetary Institute Science Conference Abstracts*, page 1888, March.
- Daly, T., P. Gavin, and V. Chevrier (2011), Effects of thermal alteration on the near-infrared and mid-infrared spectra of Martian phyllosilicates. In *Lunar and Planetary Institute Science Conference Abstracts*, volume 42 of *Lunar and Planetary Institute Science Conference Abstracts*, page 1164, March.
- Ehlmann, B. L., J. F. Mustard, C. I. Fassett, S. C. Schon, J. W. Head, III, D. J. Des Marais, J. A. Grant, and S. L. Murchie (2008a), Clay minerals in delta deposits and organic preservation potential on Mars, *Nat. Geosci.*, 1, 355–358, doi:10.1038/ngeo207.
- Ehlmann, B. L. et al. (2008b), Orbital Identification of carbonate-bearing rocks on Mars, *Science*, 322, 1828, doi:10.1126/science.1164759.
- Ehlmann, B. L., et al. (2009), Identification of hydrated silicate minerals on Mars using MRO-CRISM: Geologic context near Nili Fossae and implications for aqueous alteration, *J. Geophys. Res.*, 114, E00D08, doi:10.1029/2009JE003339.
- Ehlmann, B. L., J. F. Mustard, and S. L. Murchie (2010), Geologic setting of serpentine deposits on Mars, *Geophys. Res. Lett.*, 37, L06201, doi:10.1029/2010GL042596.
- Ehlmann, B. L., J. F. Mustard, S. L. Murchie, J.-P. Bibring, A. Meunier, A. A. Fraeman, and Y. Langevin (2011a), Subsurface water and clay mineral formation during the early history of Mars, *Nature*, 479, 53–60, doi:10.1038/nature10582.
- Ehlmann, B. L., J. F. Mustard, R. N. Clark, G. A. Swayze, and S. L. Murchie (2011b), Evidence for low-grade metamorphism, hydrothermal alteration, and diagenesis on Mars from phyllosilicate mineral assemblages, *Clays Clay Miner.*, 59(4), 359–377, doi:10.1346/CCMN.2011.0590402. URL <http://ccm.geoscienceworld.org/content/59/4/359.abstract>
- Farrand, W. H., L. R. Gaddis, and L. Keszthelyi (2005), Pitted cones and domes on Mars: Observations in Acidalia Planitia and Cydonia Mensae using MOC, THEMIS, and TES data, *J. Geophys. Res.*, 110, E05005, doi:10.1029/2004JE002297.
- Farrand, W. H., T. D. Glotch, J. W. Rice, J. A. Hurowitz, and G. A. Swayze (2009), Discovery of jarosite within the Mawrth Vallis region of Mars: Implications for the geologic history of the region, *Icarus*, 204, 478–488, doi:10.1016/j.icarus.2009.07.014.
- Fassett, C. I., and J. W. Head (2008a), The timing of Martian valley network activity: Constraints from buffered crater counting, *Icarus*, 195, 61–89, doi:10.1016/j.icarus.2007.12.009.
- Fassett C. I., and J. W. Head (2008b), Valley network-fed, open-basin lakes on Mars: Distribution and implications for Noachian surface and subsurface hydrology, *Icarus*, 198, 37–56, doi:10.1016/j.icarus.2008.06.016.
- Fassett, C. I., and J. W. Head (2011), Sequence and timing of conditions on early Mars, *Icarus*, 211, 1204–1214, doi: 10.1016/j.icarus.2010.11.014.
- Frey, M., and D. Robinson (1998), *Low-Grade Metamorphism*, Wiley-Blackwell, New York.
- Gaidos, E., and G. Marion (2003), Geological and geochemical legacy of a cold early Mars, *J. Geophys. Res.*, 108, 5055, doi:10.1029/2002JE002000.
- Gaudin, A., E. Dehouck, and N. Mangold (2011), Evidence for weathering on early Mars from a comparison with terrestrial weathering profiles, *Icarus*, 216, 257–268, doi:10.1016/j.icarus.2011.09.004.
- Gavin, P., and V. Chevrier (2010), Thermal alteration of nontronite and montmorillonite: Implications for the Martian surface, *Icarus*, 208, 721–734, doi:10.1016/j.icarus.2010.02.027.
- Gavin, P., V. Chevrier, K. Ninagawa, A. Gucsik, and S. Hasegawa (2011), Experimental Investigation into the effects of meteoritic impacts on the near- and mid-infrared spectra of Martian phyllosilicates. In *Lunar and Planetary Institute Science Conference Abstracts*, volume 42 of *Lunar and Planetary Institute Science Conference Abstracts*, page 1921, March.
- Gendrin, A., et al. (2005), Sulfates in Martian layered terrains: The OMEGA/Mars Express view, *Science*, 307, 1587–1591, doi:10.1126/science.1109087.
- Golombek, M., et al. (2012), Selection of the Mars Science Laboratory landing site, *Space Sci. Rev.*, 170, 641–737, doi:10.1007/s11214-012-9916-y.
- Golombek, M. P., and N. T. Bridges (2000), Erosion rates on Mars and implications for climate change: Constraints from the Pathfinder landing site, *J. Geophys. Res.*, 105, 1841–1854, doi:10.1029/1999JE001043.
- Goudge, T. A., J. W. Head, J. F. Mustard, and C. I. Fassett (2012), An analysis of open-basin lake deposits on Mars: Evidence for the nature of associated lacustrine deposits and post-lacustrine modification processes, *Icarus*, 219, 211–229, doi:10.1016/j.icarus.2012.02.027.
- Gross, C., L. Wendt, J.-P. Combe, P. Jodkowski, G. A. Marzo, T. L. Roush, T. McCord, P. Halbach, and G. Neukum (2012), Investigating the phyllosilicate bearing Micoud crater in the northern plains of Mars. In *Lunar and Planetary Institute Science Conference Abstracts*, volume 43 of *Lunar and Planetary Institute Science Conference Abstracts*, page 1795, March.
- Hanley, J., V. F. Chevrier, J. B. Dalton, and C. S. Jamieson (2011), Reflectance spectra of low-temperature chloride and perchlorate hydrates relevant to planetary remote sensing. In *Lunar and Planetary Institute Science Conference Abstracts*, volume 42 of *Lunar and Planetary Institute Science Conference Abstracts*, page 2327, March.
- Hartmann, W. K. (2005), Martian cratering 8: Isochron refinement and the chronology of Mars, *Icarus*, 174, 294–320, doi:10.1016/j.icarus.2004.11.023.
- Hynek, B. M., M. Beach, and M. R. T. Hoke (2010), Updated global map of Martian valley networks and implications for climate and hydrologic processes, *J. Geophys. Res.*, 115, E09008, doi:10.1029/2009JE003548.
- Irwin, R. P., A. D. Howard, R. A. Craddock, and J. M. Moore (2005), An intense terminal epoch of widespread fluvial activity on early Mars: 2. Increased runoff and paleolake development, *J. Geophys. Res.*, 110, E12S15, doi:10.1029/2005JE002460.
- Langevin, Y., F. Poulet, J.-P. Bibring, and B. Gondet (2005), Sulfates in the north polar region of Mars detected by OMEGA/Mars Express, *Science*, 307, 1584–1586, doi:10.1126/science.1109091.
- Le Deit, L., J. Flahaut, C. Quantin, E. Hauber, D. Mège, O. Bourgeois, J. Gurgurewicz, M. Massé, and R. Jaumann (2012), Extensive surface pedogenic alteration of the Martian Noachian crust suggested by plateau phyllosilicates around Valles Marineris, *J. Geophys. Res.*, 117, E00J05, doi:10.1029/2011JE003983.
- Loizeau, D., et al. (2007), Phyllosilicates in the Mawrth Vallis region of Mars, *J. Geophys. Res.*, 112, E08S08, doi:10.1029/2006JE002877.
- Loizeau, D., N. Mangold, F. Poulet, V. Ansan, E. Hauber, J.-P. Bibring, B. Gondet, Y. Langevin, P. Masson, and G. Neukum (2010), Stratigraphy in the Mawrth Vallis region through OMEGA, HRSC color imagery and DTM, *Icarus*, 205, 396–418, doi:10.1016/j.icarus.2009.04.018.
- Loizeau, D., J. Carter, S. Bouley, N. Mangold, F. Poulet, J.-P. Bibring, F. Costard, Y. Langevin, B. Gondet, and S. L. Murchie (2012), Characterization of hydrated silicate-bearing outcrops in Tyrrhena Terra, Mars: Implications to the alteration history of Mars, *Icarus*, 219, 476–497, doi:10.1016/j.icarus.2012.03.017, in press.
- Mangold, N., et al. (2007), Mineralogy of the Nili Fossae region with OMEGA/Mars Express data: 2. Aqueous alteration of the crust, *J. Geophys. Res.*, 112, E08S04, doi:10.1029/2006JE002835.
- Mangold, N. (2012), Fluvial landforms on fresh impact ejecta on Mars, *Planet. Space Sci.*, 62, 69–85, doi:10.1016/j.pss.2011.12.009.
- Mangold, N., A. Gendrin, B. Gondet, S. Le Mouélic, C. Quantin, V. Ansan, J.-P. Bibring, Y. Langevin, P. Masson, and G. Neukum (2008), Spectral and geological study of the sulfate-rich region of West Candor Chasma, Mars, *Icarus*, 194, 519–543, doi:10.1016/j.icarus.2007.10.021.
- Mangold, N., L. Roach, R. Milliken, S. Le Mouélic, V. Ansan, J. P. Bibring, P. Masson, J. F. Mustard, S. Murchie, and G. Neukum (2010), A Late Amazonian alteration layer related to local volcanism on Mars, *Icarus*, 207, 265–276, doi:10.1016/j.icarus.2009.10.015.
- Mangold, N., S. Adeli, S. Conway, V. Ansan, and B. Langlais (2012), A chronology of early Mars climatic evolution from impact crater degradation, *J. Geophys. Res.*, 117, E04003, doi:10.1029/2011JE004005, in press.
- Marzo, G. A., A. F. Davila, L. L. Tornabene, J. M. Dohm, A. G. Fairén, C. Gross, T. Kneissl, J. L. Bishop, T. L. Roush, and C. P. McKay (2010), Evidence for Hesperian impact-induced hydrothermalism on Mars, *Icarus*, 208, 667–683, doi:10.1016/j.icarus.2010.03.013.
- Massé, M., S. Le Mouélic, O. Bourgeois, J.-P. Combe, L. Le Deit, C. Sotin, J.-P. Bibring, B. Gondet, and Y. Langevin (2008), Mineralogical composition, structure, morphology, and geological history of Aram Chaos crater fill on Mars derived from OMEGA Mars Express data, *J. Geophys. Res.*, 113, E12006, doi:10.1029/2008JE003131.
- Massé, M., O. Bourgeois, S. Le Mouélic, C. Verpoorter, L. Le Deit, and J. P. Bibring (2010), Martian polar and circum-polar sulfate-bearing deposits: Sublimation tills derived from the North Polar Cap, *Icarus*, 209, 434–451, doi:10.1016/j.icarus.2010.04.017.
- McGill, G. E. (2002), The small domes and pits of Cydonia Mensae and adjacent Acidalia Planitia, Mars: Implications for the role of near-surface water or ice. In *Lunar and Planetary Institute Science Conference Abstracts*, volume 33 of *Lunar and Planetary Inst. Technical Report*, page 1126, March.
- McGuire, P. C., et al. (2009), An improvement to the volcano-scan algorithm for atmospheric correction of CRISM and OMEGA spectral data, *Planetary and Space Science*, 57, 809–815, doi:10.1016/j.pss.2009.03.007.

- McKeown, N. K., J. L. Bishop, E. Z. Noe Dobrea, B. L. Ehlmann, M. Parente, J. F. Mustard, S. L. Murchie, G. A. Swayze, J.-P. Bibring, and E. A. Silver (2009), Characterization of phyllosilicates observed in the central Mawrth Vallis region, Mars, their potential formational processes, and implications for past climate, *J. Geophys. Res.*, *114*, E00D10, doi:10.1029/2008JE003301.
- Meunier, A., S. Petit, C. S. Cockell, A. El Albani, and D. Beaufort (2010), The Fe-rich clay microsystems in basalt-komatiite lavas: Importance of Fe-smectites for pre-biotic molecule catalysis during the Hadean Eon, *Orig. Life Evol. Biosph.*, *40*, 253–272, doi:10.1007/s11084-010-9205-2.
- Michalski, J. R., M. D. Kraft, T. G. Sharp, L. B. Williams, and P. R. Christensen (2005), Mineralogical constraints on the high-silica Martian surface component observed by TES, *Icarus*, *174*, 161–177, doi:10.1016/j.icarus.2004.10.022.
- Michalski, J. R., M. D. Kraft, T. G. Sharp, L. B. Williams, and P. R. Christensen (2006), Emission spectroscopy of clay minerals and evidence for poorly crystalline aluminosilicates on Mars from Thermal Emission Spectrometer data, *J. Geophys. Res.*, *111*, E03004, doi:10.1029/2005JE002438.
- Michalski, J., F. Poulet, J.-P. Bibring, and N. Mangold (2010), Analysis of phyllosilicate deposits in the Nili Fossae region of Mars: Comparison of TES and OMEGA data, *Icarus*, *206*, 269–289, doi:10.1016/j.icarus.2009.09.006.
- Milliken, R. E., and D. L. Bish (2010), Sources and sinks of clay minerals on Mars, *Philos. Mag.*, *90*, 2293–2308, doi:10.1080/14786430903575132.
- Milliken, R. E., et al. (2008), Opaline silica in young deposits on Mars, *Geology*, *36*, 847–850.
- Milliken, R. E., D. L. Bish, T. Bristow, and J. F. Mustard (2010), The case for mixed-layered clays on Mars. In *Lunar and Planetary Institute Science Conference Abstracts*, volume 41 of *Lunar and Planetary Institute Science Conference Abstracts*, page 2030, March.
- Morris, R. V., D. C. Golden, D. W. Ming, T. G. Graff, R. E. Arvidson, S. M. Wiseman, K. A. Lichtenberg, and S. Cull (2009), Visible and near-IR reflectance spectra for smectite, sulfate, and perchlorate under dry conditions for interpretation of Martian surface mineralogy. In *Lunar and Planetary Institute Science Conference Abstracts*, volume 40 of *Lunar and Planetary Institute Science Conference Abstracts*, page 2317, March.
- Morris, R. V., T. G. Graff, C. N. Achilles, D. A. Agresti, D. W. Ming, and D. C. Golden (2011), Visible and near-IR reflectance spectra of Mars analogue materials under arid conditions for interpretation of Martian surface mineralogy. In *Lunar and Planetary Institute Science Conference Abstracts*, volume 42 of *Lunar and Planetary Institute Science Conference Abstracts*, p. 2757, March.
- Murchie, S., et al. (2007), Compact Reconnaissance Imaging Spectrometer for Mars (CRISM) on Mars Reconnaissance Orbiter (MRO), *J. Geophys. Res.*, *112*, E05S03, doi:10.1029/2006JE002682.
- Murchie, S. L., et al. (2009), A synthesis of Martian aqueous mineralogy after 1 Mars year of observations from the Mars Reconnaissance Orbiter, *J. Geophys. Res.*, *114*, E00D06, doi:10.1029/2009JE003342.
- Mustard, J. F., et al. (2008), Hydrated silicate minerals on Mars observed by the Mars Reconnaissance Orbiter CRISM instrument, *Nature*, *454*, 305–309, doi:10.1038/nature07097.
- Noe Dobrea, E. Z., et al. (2010), Mineralogy and stratigraphy of phyllosilicate-bearing and dark mantling units in the greater Mawrth Vallis/west Arabia Terra area: Constraints on geological origin, *J. Geophys. Res.*, *115*, E00D19, doi:10.1029/2009JE003351.
- Ody, A., F. Poulet, Y. Langevin, J.-P. Bibring, G. Bellucci, F. Altieri, B. Gondet, M. Vincendon, J. Carter, and N. Manaud (2012), Global maps of anhydrous minerals at the surface of Mars from OMEGA/MEX, *J. Geophys. Res.*, *117*, E00J14, doi:10.1029/2012JE004117.
- Allen, P. A. (2009), Front matter, pages i–xi. Blackwell Science Ltd, ISBN 9781444313574. doi:10.1002/9781444313574.fmatter. URL <http://dx.doi.org/10.1002/9781444313574.fmatter>
- Pieters, C. M. (2010), Reflectance experiment laboratory (relab), <http://www.planetary.brown.edu/relab/>
- Poulet, F., J.-P. Bibring, J. F. Mustard, A. Gendrin, N. Mangold, Y. Langevin, R. E. Arvidson, B. Gondet, and C. Gomez (2005), Phyllosilicates on Mars and implications for early Martian climate, *Nature*, *438*, 623–627, doi:10.1038/nature04274.
- Poulet, F., C. Gomez, J.-P. Bibring, Y. Langevin, B. Gondet, P. Pinet, G. Bellucci, and J. Mustard (2007), Martian surface mineralogy from Observatoire pour la Mineralogie, l'Eau, les Glaces et l'Activite on board the Mars Express spacecraft (OMEGA/MEX): Global mineral maps, *J. Geophys. Res.*, *112*, E08S02, doi:10.1029/2006JE002840.
- Poulet, F., D. W. Beaty, J.-P. Bibring, D. Bish, J. L. Bishop, E. Noe Dobrea, J. F. Mustard, S. Petit, and L. H. Roach (2009), Key scientific questions and key investigations from the First International Conference on Martian Phyllosilicates, *Astrobiology*, *9*, 257–267, doi:10.1089/ast.2009.0335.
- Roach, L. H. (2009), Sulfates in Valles Marineris as indicators of the aqueous evolution of Mars. PhD thesis, Brown University.
- Ruff, S. W., and P. R. Christensen (2002), Bright and dark regions on Mars: Particle size and mineralogical characteristics based on Thermal Emission Spectrometer data, *J. Geophys. Res.*, *107*, 5127, doi:10.1029/2001JE001580.
- Schwenzer, S. P., and D. A. Kring (2009), Impact-generated hydrothermal systems capable of forming phyllosilicates on Noachian Mars, *Geology*, *37*(12), 1091–1094, doi:10.1130/G30340A.1. URL <http://geology.gsapubs.org/content/37/12/1091.abstract>
- Scott, D., and K. Tanaka (1986), Geologic map of Mars, i-1802-abc. U.S. Geological Survey Scientific Investigations Map.
- Skok, J. R., J. F. Mustard, B. L. Ehlmann, R. E. Milliken, and S. L. Murchie (2010), Silica deposits in the Nili Patera caldera on the Syrtis Major volcanic complex on Mars, *Nat. Geosci.*, *3*, 838–841, doi:10.1038/ngeo990.
- S. W., Squyres (2008), Detection of silica-rich deposits on Mars, *Science*, *320*, 1063, doi:10.1126/science.1155429.
- Swayze, G. A., et al. (2008), Discovery of the acid-sulfate mineral alunite in Terra Sirenum, Mars, using MRO CRISM: Possible evidence for acid-saline lacustrine deposits? *AGU Fall Meeting Abstracts*, page A4, December.
- Tanaka, K. L., G. J. Leonard (1995), Geology and landscape evolution of the Hellas region of Mars, *J. Geophys. Res.*, *100*, 5407–5432, doi:10.1029/94JE02804.
- Tanaka, K. L., N. K. Isbell, D. H. Scott, R. Greeley, and J. E. Guest (1988), The resurfacing history of Mars: A synthesis of digitized, Viking-based geology. In *Lunar and Planetary Science Conference Proceedings*, volume 12 of *Lunar and Planetary Science Conference Proceedings*, pages 665–678.
- Tanaka, K. L., J. A. Skinner, T. M. Hare, T. Joyal, and A. Wenker (2003), Resurfacing history of the northern plains of Mars based on geologic mapping of Mars Global Surveyor data, *J. Geophys. Res.*, *108*, 8043, doi:10.1029/2002JE001908.
- Tanaka, K. L., J. A. Skinner, and T. M. Hare (2005), Geological map of the northern plains of Mars (1:15,000,000), USGS, <http://pubs.usgs.gov/sim/2005/2888/s/>.
- Tanaka, K. L., J. M. Dohm, C. M. Fortezzo, R. P. Irwin, E. J. Kolb, J. A. Skinner, T. M. Hare, T. Platz, G. Michael, and S. Robbins (2012), The geology of Mars: What the new global map shows. In *Lunar and Planetary Institute Science Conference Abstracts*, volume 43 of *Lunar and Planetary Inst. Technical Report*, page 2702, March.
- Thollot, P., N. Mangold, V. Ansan, S. Le Mouélic, R. E. Milliken, J. L. Bishop, C. M. Weitz, L. H. Roach, J. F. Mustard, and S. L. Murchie (2012), Most Mars minerals in a nutshell: Various alteration phases formed in a single environment in Noctis Labyrinthus, *J. Geophys. Res.*, *117*, E00J06, doi:10.1029/2011JE004028.
- Tosca, N. J., and A. H. Knoll (2009), Juvenile chemical sediments and the long term persistence of water at the surface of Mars, *Earth Planet. Sci. Lett.*, *286*, 379–386, doi:10.1016/j.epsl.2009.07.004.
- Velde, B. (2010), Origin and mineralogy of clays: Clays and the environment, Springer, ISBN 3642081959.
- Vincendon, M., Y. Langevin, F. Poulet, A. Pommerol, M. Wolff, J.-P. Bibring, B. Gondet, and D. Jouglet (2009), Yearly and seasonal variations of low albedo surfaces on Mars in the OMEGA/MEX data set: Constraints on aerosols properties and dust deposits, *Icarus*, *200*, 395–405, doi:10.1016/j.icarus.2008.12.012.
- Wray, J. J., S. W. Squyres, L. H. Roach, J. L. Bishop, J. F. Mustard, and E. Z. Noe Dobrea (2010), Identification of the Ca-sulfate bassanite in Mawrth Vallis, Mars, *Icarus*, *209*, 416–421, doi:10.1016/j.icarus.2010.06.001.